Alma Mater Studiorum · University of Bologna

School of Science
Department of Physics and Astronomy
Master Degree in Physics

Exploring rich dark sectors for dark matter and neutrino masses with phenomenology at ICARUS

Supervisor:
Prof. Silvia Pascoli

Co-supervisor:
Dr. Alessandro Granelli

Submitted by:
Giuseppe Cordella

Academic Year 2022/2023

Abstract

In this master's thesis, realisations of rich dark sector models are proposed as a solution to the problems of dark matter and neutrino mass generation. In these models, sub-GeV dark photons Z' can decay into final states with both visible and invisible particles. A variable number of heavy neutral particles ψ_i is postulated, which can be treated as dark matter (DM) candidates or heavy neutral leptons giving rise to neutrino masses via seesaw mechanism. After providing extensive context, the full mass spectrum is studied with the aim of reconstructing the Yukawa couplings from observed neutrino parameters. The models are then interpreted as variations of inelastic DM (iDM) and the case is made for their testability at ICARUS experiment, in its current operation in the Fermilab Short-Baseline Neutrino program, through the decay chain $Z' \to \psi_1(\psi_2 \to \psi_1 \ell^+ \ell^-)$, with the Z' produced in rare neutral kaon decays. The parameter space region probed by this experiment is confronted with the cosmological range required for iDM. A Monte Carlo simulation (written using the `Pythia` generator and a combination of `Mathematica` and `Python` codes) was run to calculate the expected number of events in the detector. The simulation accounts for production, propagation and decay in the laboratory frame, taking into account the calculated decay rates and the geometry of the experimental setup.

Contents

Introduction

Despite its outstanding successes, the Standard Model of particle physics has proved itself unsatisfactory on two main fronts, namely the problem of dark matter and neutrino physics.
Dark matter is a reasonable hypothesis, arisen in cosmology, that justifies a number of astrophysical observations, namely the mass distribution of galaxies and galaxy clusters and the temperature fluctuations of the cosmic microwave background. The accepted cosmology paradigm, based on General Relativity, leads to the conclusion that less than 5% of the energy content of our Universe comes from visible sources, while the rest is to be split between a form of energy responsible for the accelerated expansion of the Universe (dark energy) and an invisible massive source (dark matter). The Standard Model does not include any convincing particle candidate for the latter.
As for neutrinos, they can be probably considered the least understood elementary particles: their mass is still unknown, although it is known that it cannot be zero for all three known species, and we have no evidence on whether they are identical to or different from their antiparticles (i.e. whether their nature is that of Majorana or Dirac fermions). These two questions are actually intertwined and both theoretical and experimental efforts are directed towards providing answers beyond the Standard Model.
Dark sectors lie at the crossroads between the aforementioned unsolved problems in astroparticle physics, and they are potentially capable of addressing several other issues, like low-energy anomalies and baryogenesis. They constitute a flexible theoretical framework with a fair economy of hypotheses, which invariably includes a particle content in the mass range going from a few MeV to a few GeV, communicating very feebly with the known Standard Model particles. One of their greatest advantages is that the energy range is at current reach of many experiments, even though detection events have to be rare by construction, and discerning signals from backgrounds is a significant challenge most of the time.
This work is aimed towards exploring next-to-minimal dark sector models, which contain an additional $U(1)_D$ gauge symmetry and a varying number of neutral fermions. On the theoretical side, we compute the mass spectrum of the new fermions and systematically discuss the conditions for implementing a seesaw mechanism that explains the observed neutrino mass-squared differences, compatibly with flavour mixing angles. On a phenomenological perspective, we derive the decay rates in view of testing the parameter space in a realistic setting, represented by the ICARUS experiment at Fermilab. In particular, we examine the region of cosmological interest to establish a benchmark and run a Monte Carlo simulation of the production, propagation and decay of dark sector particles in this setting, whose final result is the expected number of events.
Chapter 1 presents an overview of dark matter, presenting dark sectors as an alternative to the WIMP paradigm in the thermal picture. Chapter 2 then motivates them as providing the missing pieces to other beyond Standard Model puzzles and gives a review

of portals, i.e. the terms in the Lagrangian that provide communication with the Standard Model, focusing on a basic example of kinetic mixing model. Chapter 3 deals with the theory of rich dark sector models. First, the semi-visible dark photon models are presented and neutrino mass generation is discussed. Then we motivate their relevance for dark matter, reviewing the studies in this regard. In the last chapter we discuss the phenomenology at ICARUS and clarify how the neutral mesons produced in beam dump experiments can be used to test our models.

Chapter 1

The particle physics approach to dark matter

This chapter serves as a brief overview of the extensive field of study that is Dark Matter (DM), from the point of view of particle physics. After stating the main problems we face within our current understanding of matter at galactic scale and beyond, we will narrow the scope of the proposed solutions down to the framework of particles, and in particular to those in the mass range between the keV and the tens of GeV, which can be included in the standard thermal history of the Universe. Justification for following this road will be provided, which will hopefully convince the reader of the rising attractiveness of this approach over the others. The theoretical discussion will be integrated with a summary of the experimental attempts at finding said particles, which employ different techniques to explore the parameter spaces of the proposed models.

1.1 Observational evidence for dark matter

One of the most fascinating tasks in contemporary physics is to clarify the origin and composition of the matter content of the Universe. Since the last century it has become increasingly clearer that ordinary, visible matter, made mostly of baryons, is neither the only component, nor the most abundant.
Astrophysics is what first sparked interest in the question. Historically, observations of the motion of celestial bodies in the Solar System which were inconsistent with the understanding of the time either lead to the discovery of previously unseen objects (like the planet Neptune), or prompted the formulation of a new theory (General Relativity). Moving to galaxies and clusters, new inconsistencies arose. The name 'dark matter' was famously used in its contemporary sense by F. Zwicky in 1933 [1]: he observed the velocity dispersion of galaxies in the Coma cluster and concluded that the mass density of the visible matter in it was too low to keep the cluster gravitationally bound. Some kind of additional matter, which interacted with the ordinary one through gravity alone, could explain the missing mass.
This was confirmed in the 1970s by the measurements of galaxy rotation curves (among others, one should mention V. Rubin's distinguished works [2]). In short, Newton's law of universal gravitation predicts that the velocity v of a star at a distance r from the center of a galaxy should be

$$v = \sqrt{\frac{GM}{r}}, \tag{1.1}$$

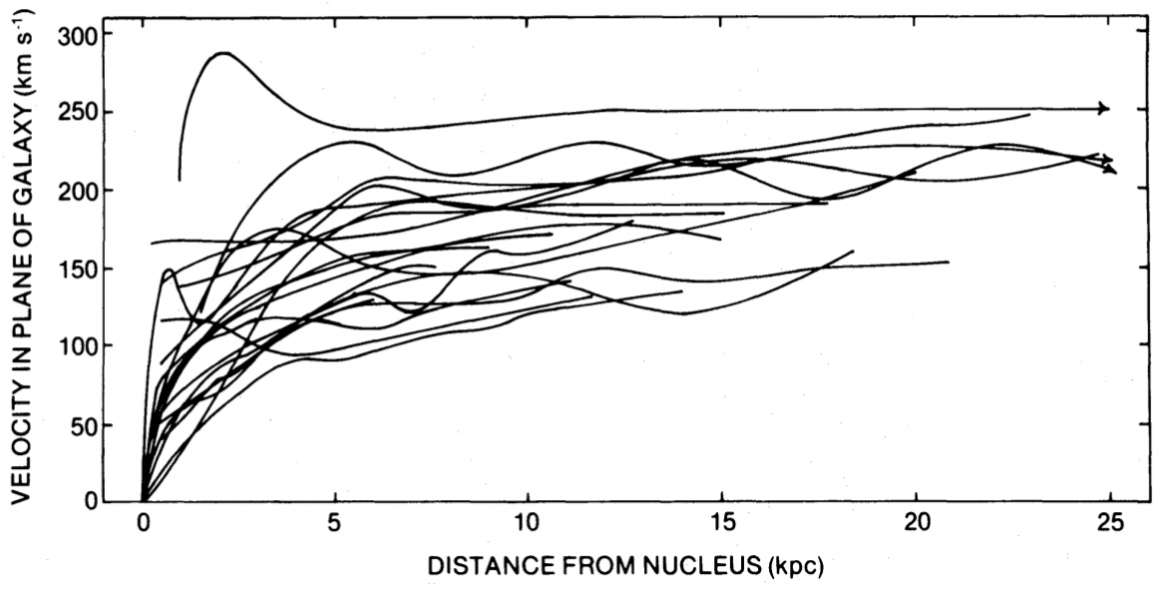

Figure 1.1: Superposition of the rotation curves of twenty-one Sc galaxies, with varying luminosities and radii. Figure taken from [2].

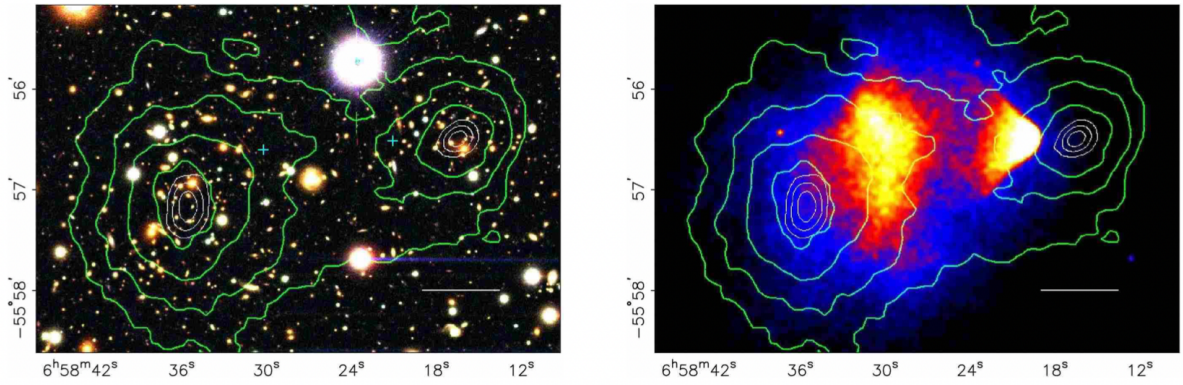

Figure 1.2: Bullet cluster 1E065-558, colour image (Magellan telescopes, left) and X-ray image (Chandra observatory, right). The white bar indicates 200 kpc at the distance of the cluster. Reconstructed gravitational lensing is contoured in green. Figure taken from [3].

where G is Newton's gravitational constant, and M is the mass within the orbit, which can be considered constant at the outer rim of the (visible) galactic disk. This $r^{-1/2}$ behaviour is not observed; rather, the velocity stays roughly constant as a function of the distance, as illustrated in figure 1.1. This can be explained by an increase of the mass $M \propto r$, that is to say, by the presence of invisible matter. Elaborating the data, with the aid of N-body simulations, it appears that this matter is distributed, with various possible density profiles, as a spherical halo extending around ten times beyond the visible galactic disk.

Additional evidence comes from gravitational lensing, i.e. the bending of light trajectories in the presence of a large mass, as described by General Relativity. In 1995 the Bullet

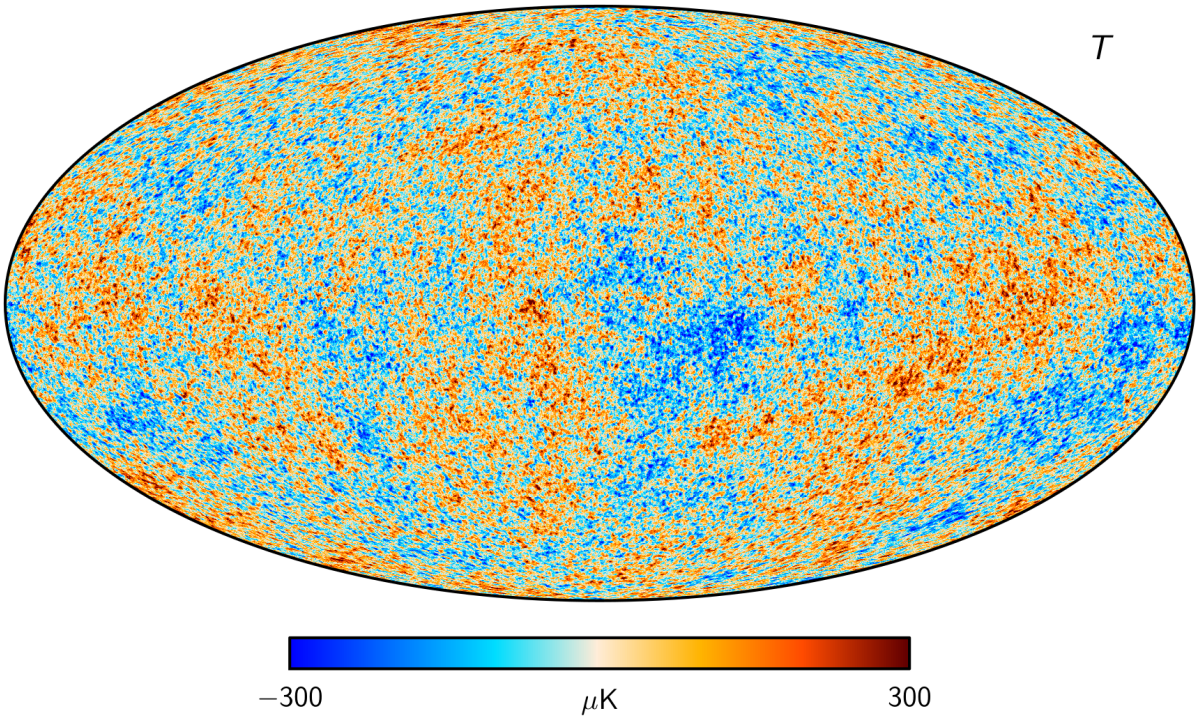

Figure 1.3: The temperature anisotropies of the CMB as observed by Planck. Tiny fluctuations correspond to density variations ultimately responsible for the structure of the Universe. Image: ESA and the Planck Collaboration.

cluster was observed, and a misalignment between the X-ray contour, coming from intergalactic ionised gas, and the gravitational field profile, tracked by gravitational lensing, was found [3] (fig. 1.3). The interpretation of data showed that its two subclusters are drifting away from each other, with the baryonic gas components moving slower than the dark component, due to the electromagnetic interaction of the gas particles.
As for cosmology, the current parametrisation of the Big Bang model must include a matter component alongside the visible one to account for the observed Cosmic Microwave Background (CMB) temperature anisotropies [4], as well as to justify the large-scale structure of the Universe resulting from surveys of the sky. This final piece of evidence leads us away from identifying (all of) the invisible matter with neutrinos. Indeed, neutrinos would seem to be a good suspect: they do interact only gravitationally over astronomical distances, being otherwise almost collisionless apart from the short-range weak interaction. Nonetheless, cosmic neutrinos are too fast to account for the observed density of large-scale structures [5]. The only solution, if we are to interpret DM in terms of particles, as we shall try throughout this work, is to turn to physics beyond the Standard Model and concoct new, plausible particle models to test. However, it is fair to say that DM could be constituted of more than one component, and that even the possibility to partially explain the above phenomena through alternative routes, like modified theories of gravity, is not ruled out completely.
Data from Planck collaboration (2018) sets DM as the second biggest contribution to the energy density of the Universe with 26%, compared to 69% for Dark Energy and 5% for

Figure 1.4: A mind-map diagram of the possible solutions to the dark matter problem. Figure taken from [6].

baryonic (ordinary) matter [4]. These three components make up the ΛCDM model,[1] which reasonably explains the CMB, the distribution of galaxies, the relative abundances of light elements and the accelerating expansion of the Universe.

1.2 Properties of particle candidates

Generally speaking, the particles constituting DM can be seen as a leftover from the events occurred in the early stages of the Universe. The fields that describe them, through some mechanism, achieved a nontrivial configuration, with a relic density we can deduce today from observations. We will make the case for one such mechanism in the following section. For now, we list all the key properties that a good DM candidate should possess.

- It should be electrically neutral or with a tiny charge.

[1] Λ stands for cosmological constant, the term in Einstein field equations identified with a form of Dark Energy, and CDM is for cold dark matter, i.e. DM slow enough to explain the observed structures.

- It should have no colour charge.
- Self-interactions should be fairly weak (due to DM being collisionless).
- It should be nonrelativistic (or nearly so in the case of a sub-eV component).
- It should be stable, or at least long-lived.

Besides satisfying these conditions, candidates are required to be compatible with Big Bang nucleosynthesis, stellar evolution and gamma ray observations, and, of course, they must be testable.
Basic quantum mechanical considerations lead to lower bounds for bosonic and fermionic DM particle masses. The smallest known distance scale at which DM is gravitationally bound is that of dwarf galaxies. Stellar kinematics shows that, for the reasons clarified in section 1.1, a dwarf galaxy should have a spherical DM halo of radius $R_{\text{halo}} \sim 1$ kpc; the average velocity of orbiting bodies at the edge, deduced from Newton's law of gravitation as in (1.1), is $v \sim 100$ km/s.
For bosonic DM, the only bound for the stability of the halo is the uncertainty principle $\Delta x \Delta p \gtrsim 1$. Taking $\Delta x \sim 2R_{\text{halo}}$ and $\Delta p \sim m_{\text{B}} v$, where m_{B} is the mass of the candidate boson, we get

$$m_{\text{B}} \gtrsim 10^{-22} \text{ eV}. \tag{1.2}$$

A tighter bound exists for fermionic DM, due to the Pauli exclusion principle. The mass of the halo can be written in terms of its volume and density as $M_{\text{halo}} = V\rho_{\text{F}}$. Expressing the density in terms of the phase space distribution function $f(p)$ of fermion gas, in nonrelativistic regime, we get

$$M_{\text{halo}} = m_{\text{F}} V \int f(p)\, \mathrm{d}^3 p \leq m_{\text{F}} V \int \mathrm{d}^3 p = m_{\text{F}} V (m_{\text{F}} v)^3, \tag{1.3}$$

where m_{F} is the mass of the candidate fermion. The inequality is made using the fact that no more than one fermion can occupy the same momentum eigenstate. Using the volume of a sphere of radius R_{halo}, and $M_{\text{halo}} \sim 10^5\, M_\odot$, we get $m_{\text{F}} \gtrsim 10$ eV. More refined estimates [7] tighten this constraint to

$$m_{\text{F}} \gtrsim 0.1 \text{ keV}. \tag{1.4}$$

This is known as the Tremaine-Gunn bound; astrophysical considerations suggest more severe bounds [8].
As for the upper bound, for composite DM coming in clumps, the integrity of bound compact systems like globular clusters upon interaction with DM requires the mass of the clumps not to exceed $10^3\, M_\odot$, or 10^{70} eV [9]. This gives an enormous mass range to deal with. In any case, elementary DM particles cannot be heavier than the Planck mass $m_{\text{P}} \sim 10^{28}$ eV, at which quantum effects of gravity become significant.

1.3 The thermal picture

The most frequently invoked mechanism for the origin of DM relics is thermal freeze out. There are multiple reasons for that. First, it is the same mechanism that all Standard Model particles (SM particles, from now on) are believed to have undergone; this provides useful milestones to the reconstructed history of the Universe. Second,

as we will see in 1.3.3, the mass range is limited to an area which is already object of extensive research, both theoretical and experimental. Candidates in this window nicely fit into extensions of the Standard Model that were developed for reasons other than DM, and seem to solve more than one problem. Finally, it is particularly interesting to see how experiments designed for apparently unrelated searches can in fact have thermal range DM signatures. This section is devoted to reviewing the basics of the freeze out mechanism, and to restricting the mass range of thermal DM candidates, through order of magnitude estimates.

Rolling back time, the expansion of the Universe suggests that, in its early history, it was much hotter and denser than it is now. Particles were close together, to the point that free motion was severely limited by the frequent collisions, which also disrupted any bound state. The picture is that of a plasma of elementary particles in thermal equilibrium, at temperature T. As the Universe expanded, it also cooled down, leaving more room to the particles and slowing them down. When the interaction probability among specific particle species, described by the cross section σ, dropped below a threshold fixed by the expansion of the Universe, those species are left to freely stream, and are therefore said to *freeze out* of the thermal bath.

To translate this idea into mathematical terms, we need two quantities. The first is the *interaction rate*

$$\Gamma = n(T)\langle\sigma v\rangle_T, \tag{1.5}$$

where n is the number density of the particle species under examination, v is the relative velocity in the collision process, and the angular bracket denotes a thermal average. The interaction rate has to be compared with the *expansion rate*, which, for the standard cosmological model, is given by the Hubble parameter

$$H = \frac{\dot{a}(t)}{a(t)}, \tag{1.6}$$

where $a(t)$ is the scale factor from Robertson-Walker metric. Equating these two quantities, we can find the approximate decoupling instant.

If we then plug this relation into an evolution equation, which expresses the number density as a function of time, we can find the density at freeze out. The latter can be directly related to the density at present time through the scale factor cubed, and compared to the observed abundance of the species. The cross section is left as an unknown, and is therefore what we will extract from this calculation. Then, using standard assumptions from scattering theory, the mass of the particle can be deduced. Schematically, to estimate the thermal DM candidate mass, the three ingredients to be put together are:

- the evolution equation (Boltzmann equation),
- the freeze out condition $\Gamma \sim H$,
- the observed DM density (in terms of the parameter $\Omega_{\rm DM}h^2 \sim 0.1$).[2]

We shall deal with this task in the ensuing subsections, following the standard reasoning found in textbooks such as [10] and [11].

[2]Data from the Planck collaboration [4] sets $\Omega_{\rm DM}h^2 = 0.315 \pm 0.007$; h is the reduced Hubble constant.

1.3.1 Boltzmann equation for the early universe

In the kinetic theory of gases, the statistical behaviour of a thermodynamic system whose components can get out of equilibrium is described by the Boltzmann equation

$$\mathbf{L}[f(x,p)] = \mathbf{C}[f(x,p)], \tag{1.7}$$

where f is the phase space distribution function. $\mathbf{L}$ is the Liouville operator, describing the evolution of phase space volumes under Hamiltonian flow, and $\mathbf{C}$ is the collision operator, which keeps track of particle interactions. The general-relativistic expression for $\mathbf{L}[f(x,p)]$ is

$$\mathbf{L}[f(x,p)] = p^\alpha \frac{\partial f}{\partial x^\alpha} - \Gamma^\alpha_{\beta\gamma} p^\beta p^\gamma \frac{\partial f}{\partial p^\alpha}. \tag{1.8}$$

For a Friedmann-Lemaître-Robertson-Walker (FLRW) universe, this reduces to

$$\mathbf{L}[f(t,E)] = E\frac{\partial f}{\partial t} - H|\mathbf{p}|^2 \frac{\partial f}{\partial E}, \tag{1.9}$$

by virtue of spatial homogeneity and isotropy. Dividing by the energy and integrating over momentum space, assuming any exponentially decaying distribution, we get an expression in terms of the number density:

$$\int \mathrm{d}^3p \frac{\mathbf{L}[f(t,E)]}{E} = \frac{\partial n}{\partial t} + 3Hn. \tag{1.10}$$

Let us deal with the collision operator. Since we have to account for the interactions of one particle species, which will decouple from the thermal bath, with other particles in the system, we assign a subscript χ to the quantities referring to that species, and latin letters to the rest. Considering a process $\chi + a + b + \cdots \to i + j + \ldots$, the collision operator, divided by E_χ and integrated over the momenta to match the steps done for the Liouville operator, has a rather cumbersome appearance:

$$\begin{aligned}\int \mathrm{d}^3p_\chi \frac{\mathbf{C}[f(t,E)]}{E_\chi} = &- \int \mathrm{d}\Pi_\chi \, \mathrm{d}\Pi_a \, \mathrm{d}\Pi_b \ldots \mathrm{d}\Pi_i \, \mathrm{d}\Pi_j \ldots \\ &\times (2\pi)^4 \delta^{(4)}(p_\chi + p_a + p_b + \ldots - p_i - p_j - \ldots) \\ &\times \left[|\mathcal{M}_{\chi+a+b+\ldots \to i+j+\ldots}|^2 f_a f_b \ldots f_\chi (1 \pm f_i)(1 \pm f_j) \ldots \right. \\ &\left. - |\mathcal{M}_{i+j+\ldots \to \chi+a+b+\ldots}|^2 f_i f_j \ldots (1 \pm f_\chi)(1 \pm f_a)(1 \pm f_b) \ldots \right]. \end{aligned} \tag{1.11}$$

Here we recognise:

- the Lorentz-invariant measure for the k-th species $\mathrm{d}\Pi_k = g_k \frac{\mathrm{d}^3 p_k}{(2\pi)^3 2E_k}$, where g_k quantifies the internal degrees of freedom;
- the S-matrix element $\mathcal{M}$ for both the direct and the inverse process;
- Bose enhancing and Fermi blocking factors $(1 \pm f_k)$ dependent on the statistics.

We can get a simplified expression by making the following assumptions:

1. time-reversal (or CP) symmetry is retained (so that the S-matrix element squared is the same for both time directions);

2. all processes save for $2 \to 2$ are suppressed;

3. we take all species to be in kinetic equilibrium, and to follow Maxwell-Boltzmann distribution $f_k \propto \mathrm{e}^{\frac{\mu_k - E_k}{T}}$, where μ_k is the chemical potential (so that $1 \pm f_k = 1$ for each k).

This way we obtain, using the integers 1 to 4 as labels for readability,

$$\int \mathrm{d}^3 p_1 \frac{\mathbf{C}[f_1(t,E)]}{E_1} = -\int \mathrm{d}\Pi_1\, \mathrm{d}\Pi_2\, \mathrm{d}\Pi_3\, \mathrm{d}\Pi_4 \times (2\pi)^4 \delta^{(4)}(p_1 + p_2 - p_3 - p_4) |\mathcal{M}|^2 \left(f_1 f_2 - f_3 f_4\right). \quad (1.12)$$

Defining n_k^{eq} as the number density of the k-th species at chemical equilibrium ($\mu_k = 0$), and therefore at full thermodynamic equilibrium, and applying energy conservation, (1.12) becomes

$$\int \mathrm{d}^3 p_1 \frac{\mathbf{C}[f_1(t,E)]}{E_1} = -\, n_1^{\mathrm{eq}} n_2^{\mathrm{eq}} \langle \sigma v \rangle \left(\frac{n_1 n_2}{n_1^{\mathrm{eq}} n_2^{\mathrm{eq}}} - \frac{n_3 n_4}{n_3^{\mathrm{eq}} n_4^{\mathrm{eq}}} \right), \quad (1.13)$$

where we have identified the thermally averaged cross section

$$\langle \sigma v \rangle = \frac{1}{n_1^{\mathrm{eq}} n_2^{\mathrm{eq}}} \int \mathrm{d}\Pi_1\, \mathrm{d}\Pi_2\, \mathrm{d}\Pi_3\, \mathrm{d}\Pi_4 (2\pi)^4 \delta^{(4)}(p_1 + p_2 - p_3 - p_4) |\mathcal{M}|^2. \quad (1.14)$$

The final step requires two further hypotheses:

4. the process is an annihilation $\chi\bar{\chi} \to \psi\bar{\psi}$, where χ is the DM particle, and ψ a SM particle (the bar denotes antiparticles);

5. the products ψ, $\bar{\psi}$ are in chemical equilibrium, and therefore in full thermodynamic equilibrium, with the bath.

Putting together (1.13) and (1.10) through (1.7), we get the final form of our evolution equation for the DM particle density n (we drop the subscript 1):

$$\frac{\partial n}{\partial t} + 3Hn = -\langle \sigma v \rangle \left(n^2 - n_{\mathrm{eq}}^2 \right). \quad (1.15)$$

The term containing the Hubble parameter accounts for the expansion of the Universe. The right-hand side expresses the balance between the direct and inverse reactions, and vanishes if there is equilibrium or no interaction.

1.3.2 Estimate of the annihilation cross section

Equation (1.15) has no closed-form analytic solution. However, there exist both a viable partial-wave expansion and precise numerical solutions. For the scope of this section, which is demonstrating how the cross section is evaluated, we will neglect the temperature dependence of $\langle \sigma v \rangle$ (s-wave approximation).
We would like to recast the evolution equation in terms of the variable $x \equiv m/T$, with m the mass of the DM particle, and of the unknown function $Y \equiv n/s$, with s the entropy per unit volume. Y is sometimes called the comoving abundance and has the purpose of factoring out the dependence on the scale factor a, as both n and s scale as a^{-3}. We

start by noticing that the left-hand side of (1.15) can be written simply as $s\frac{\mathrm{d}Y}{\mathrm{d}t}$, using entropy conservation $\frac{\mathrm{d}}{\mathrm{d}t}(sa^3) = 0$. Then, to relate time to the temperature (and then to x), we use the fact that, for a radiation-dominated universe,[3]

$$H = \sqrt{\frac{8\pi G}{3}\rho_{\mathrm{rad}}} \simeq \sqrt{\frac{8\pi G}{3}}\sqrt{\frac{\pi^2 g_*}{30}}T^2 \simeq 1.66\sqrt{g_*}\frac{T^2}{m_{\mathrm{P}}}, \tag{1.16}$$

where ρ_{rad} is the energy density and g_* is the number of effectively massless degrees of freedom, which enters the formula for ρ_{rad}. The number g_* counts the different particle species assigning statistical weights 1 to baryons and 7/8 to fermions. It can also account for relativistic species at different temperatures, like neutrinos after they decouple from the thermal bath, with appropriate weights. From (1.16), together with the relation $a \propto \sqrt{t}$, again specific of radiation domination epoch, we get

$$t \simeq 0.3\, g_*^{-1/2}\, \frac{m_{\mathrm{P}}}{T^2}. \tag{1.17}$$

With these relations at hand, the evolution equation becomes

$$\frac{\mathrm{d}Y}{\mathrm{d}x} = -\, x\frac{\langle\sigma v\rangle}{H(T=m)}s\left(Y^2 - Y_{\mathrm{eq}}^2\right). \tag{1.18}$$

We use the following expression for the entropy density, which can be considered dominated by the contribution of relativistic species:

$$s = \frac{2\pi^2}{45}g_{*s}T^3, \tag{1.19}$$

where g_{*s} again counts the particle species, but with a different weight due to the relation $s \propto T^3$ (as opposed to $\rho_{\mathrm{rad}} \propto T^4$). We then set

$$\lambda \equiv x\frac{\langle\sigma v\rangle}{H}s\bigg|_{x=1} = 0.264\,\frac{g_{*s}}{g_*}m_{\mathrm{P}}\, m\langle\sigma v\rangle, \tag{1.20}$$

which we take to be constant by virtue of the s-wave approximation. To further simplify equation (1.18), we notice that, long after the freeze-out instant ($x \gg x_{\mathrm{F}}$, where x_{F} is set by imposing $\Gamma = H$), the comoving abundance of DM particles is much larger than it was when DM was in the thermal bath. Indeed, contrary to what happens for hot relics, the equilibrium abundance follows the nonrelativistic behaviour $Y_{\mathrm{eq}} \propto x^{3/2}\mathrm{e}^{-x}$, and is therefore quickly suppressed after freeze out. This means that we can neglect Y_{eq} at the right-hand side.
Finally, we get, at late times,

$$\frac{\mathrm{d}Y}{\mathrm{d}x} \simeq -\frac{\lambda}{x^2}Y^2. \tag{1.21}$$

Integrating from x_F to infinity (present time),

$$\frac{1}{Y_\infty} - \frac{1}{Y_{\mathrm{F}}} = \frac{\lambda}{x_{\mathrm{F}}}. \tag{1.22}$$

Typically, $Y_{\mathrm{F}} \gg Y_\infty$, so that

$$Y_\infty \simeq \frac{x_{\mathrm{F}}}{\lambda}. \tag{1.23}$$

[3]The epoch we are considering for thermal freeze out. Indeed, going backwards in time, the Universe dynamics gets dominated by massless species, as $\rho_{\mathrm{rad}} \propto a^{-4}$ whereas $\rho_{\mathrm{matter}} \propto a^{-3}$ for massive species.

One can estimate the value of $x_{\rm F}$ to be around 10, for instance solving (1.18) also at early times $x \ll x_{\rm F}$ and matching the solutions in the two domains. To complete, we can compute the present-day DM density $\rho_{\rm DM} = m s_0 Y_\infty$, using the value $s_0 = 2970\,{\rm cm}^{-3}$ for the entropy density, and from that the density parameter $\Omega_{\rm DM}$. Imposing the observed value $\Omega_{\rm DM} h^2 \sim 0.1$, the cross section is found to be around $10^{-26}\,{\rm cm}^3/{\rm s}$.
More precise calculations, which include a dependence of $\langle\sigma v\rangle$ on the relative velocity (actually necessary for consistency with CMB constraints), set the desired range to

$$\langle\sigma v\rangle \simeq (2-3)\times 10^{-26}\,{\rm cm}^3/{\rm s}. \tag{1.24}$$

1.3.3 Lee-Weinberg bound and possible workarounds

The result (1.24) has been widely used as a justification for the WIMP (weakly-interacting massive particle) paradigm. As we are about to show, the preferred mass range for thermal DM nicely intersects with that of the lightest particles of supersymmetric extensions of the SM. This correspondence, known as the WIMP miracle, has bent the attention of the particle physics community towards these models for decades, as SUSY solves both theoretical issues, like the long-standing hierarchy problem, and the observational DM questions.
We start by considering a generic tree-level process $\chi\bar{\chi} \to f\bar{f}$, where f is a SM fermion, mediated by a gauge boson V, which couples with the DM particles through a coupling g_χ, and with the SM fermions through g_f:

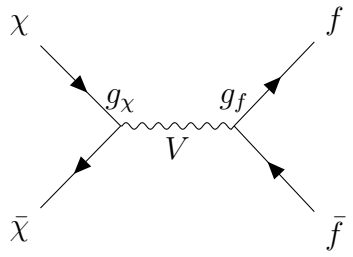

Neglecting the fermion mass, in the nonrelativistic limit we get

$$\sigma \simeq \int {\rm d}\Omega_{\rm CM} \frac{1}{v} \frac{|\mathcal{M}|^2}{32\pi^2 s} \tag{1.25}$$

where $\Omega_{\rm CM}$ is the scattering solid angle in the center of mass frame and v is the relative velocity; the center of mass energy s can be approximated, again in the nonrelativistic limit, as

$$s = E_{\rm CM}^2 = 4m_\chi^2 + O(m_\chi T). \tag{1.26}$$

This results in the thermal average being, roughly,

$$\langle\sigma v\rangle \simeq \frac{|\mathcal{M}|^2}{32\pi m_\chi^2}. \tag{1.27}$$

Now, if χ is a Dirac fermion, and V a vector mediator of mass m_V, the spin-averaged S-matrix element squared is given by

$$|\mathcal{M}|^2 \simeq g_\chi^2 g_f^2 \frac{32 m_\chi^4}{(s - m_V^2)^2}. \tag{1.28}$$

If $m_V > m_\chi$ (so that the process $\chi\bar{\chi} \to VV$ is excluded), then (1.27) becomes

$$\langle \sigma v \rangle \sim \frac{g_\chi^2 g_f^2 m_\chi^2}{\pi m_V^4}, \tag{1.29}$$

and this theoretical expression may be compared with the order of magnitude given by (1.24), which, changing units, can be written as $10^{-9}\,\mathrm{GeV}^{-2}$. This gives both an upper and lower bound for thermal candidates.
It can be shown that, requiring unitarity, an upper bound exists around 100 TeV. As for the lower bound, the standard picture assumes weak-scale couplings, leading to the electroweak scale for the DM candidate (and mediator) mass:

$$m_\chi \gtrsim 1\,\mathrm{GeV}. \tag{1.30}$$

This was discovered by Lee and Weinberg [12], and separately by other authors.
As we stated above, this range nicely overlaps with the territory of the lightest supersymmetric particle (LSP), which, in most SUSY models, is a neutral fermion with a mass around the TeV scale. Such particles should be quite easy to detect, but no positive evidence of their existence was produced at LHC (or in any other experiment). This failure has fuelled the search for alternative explanations, which relax some of the hypotheses used in the above derivations.
One interesting idea is to consider interactions that are weaker than the weak scale. Adjusting the couplings in (1.29), we see that this allows for a lighter mediator; the latter would have evaded experimental detection due to the small statistics caused by the tiny couplings. This explanation, aptly named Feebly Interacting Particles (FIPs), leaves the DM candidate mass free, down to the keV scale, below which it would be in tension with the CDM picture. FIPs are easily embedded in Dark Sectors, that will be dealt with in chapter 2. The Dark Sectors framework can include annihilation channels which are more complicated than the one illustrated above, giving rise to a diverse phenomenology. We might as well tune the masses in (1.28) to obtain a resonant behaviour and a subsequent change in relic density, but that would require a natural explanation. An enhancement in the cross section is we consider a Majorana fermion as mediator ($\langle \sigma v \rangle \propto 1/m_V^2$). Another proposal is considering cosmological circumstances that could have brought Ω_{DM} to its current value. It could be that DM annihilation stopped before the calculated freeze out time due to an asymmetry between DM particles and antiparticles, which requires a mechanism to generate it similar to baryogenesis. Or, the cosmic DM density could have dropped due to some entropy release after freeze out. We shall not explore these possibilities in the following, instead focusing on the particle contents and annihilation mechanisms in BSM pictures.

1.4 Experimental searches for thermal candidates

The search for new particles at the mass scale dictated by the WIMP paradigm and below proceeds essentially along three main roads, corresponding to the ways DM candidates can interact with SM particles:

- *direct detection*, in which one looks at the recoil of SM targets in large detectors due to interactions with the DM halo;

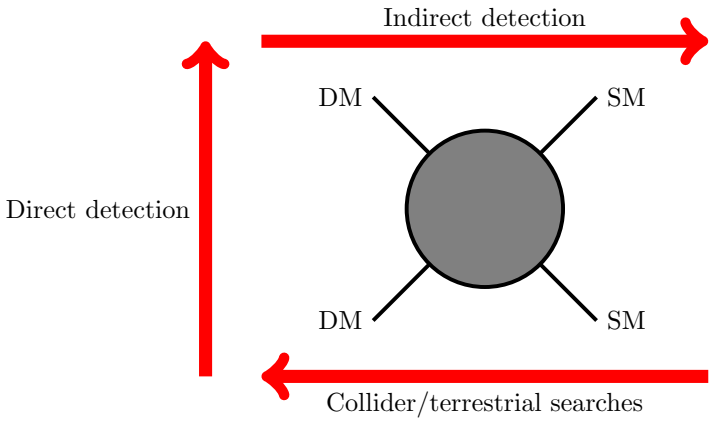

Figure 1.5: The three DM detection channels. The red arrows denote the time axis, and therefore the direction in which the diagram should be read.

- *indirect detection*, in which the SM products of the same DM annihilation processes of the early universe are looked for in regions of the sky where a large DM density is expected;
- *collider/terrestrial searches*, in which the DM candidate is produced starting from SM particles by the means of particle accelerators.

We will briefly review how these searches are usually conducted for WIMPs and lighter thermal candidates.

1.4.1 Direct detection

The idea at the foundation of direct searches is that galactic DM permeates Earth and may scatter off suitable targets, with an incoming velocity due to both its intrinsic motion and the revolution of the solar system around the center of the galaxy.

WIMP searches

The obvious choice of targets for WIMPs is atomic nuclei, as first proposed in [13], [14]. The collision of a DM particle of mass m_χ onto a nucleus of mass m_N, causes a momentum transfer $q \simeq m_\chi v$. The recoil energy of the nucleus is

$$E_{\mathrm{R}} = \frac{q^2}{2m_N} \simeq 50 \text{ keV} \left(\frac{m_\chi}{100 \text{ GeV}}\right)^2 \left(\frac{100 \text{ GeV}}{m_N}\right). \tag{1.31}$$

From standard scattering theory, the interaction rate for a flux of particles Φ entering a detector containing N_{t} targets is given by

$$R = N_{\mathrm{t}} \Phi \sigma = \frac{M_{\mathrm{det}}}{m_N} n_\chi v \sigma, \tag{1.32}$$

where M_{det} is the total mass of the detector. Differentiating with respect to the recoil energy and taking the thermal average in the velocity range available to the detector, we get

$$\frac{\mathrm{d}R}{\mathrm{d}E_{\mathrm{R}}} = \frac{\rho_\chi M_{\mathrm{det}}}{m_\chi m_N} \int_{v_{\mathrm{min}}}^{v_{\mathrm{max}}} v \tilde{f}(\mathbf{v}, t) \frac{\mathrm{d}\sigma}{\mathrm{d}E_{\mathrm{R}}} \mathrm{d}^3 v. \tag{1.33}$$

We will briefly analyse all the terms appearing in this formula. A full discussion is in [15] and references therein.

Astrophysical observables. The local DM density ρ_χ is roughly 0.3 g/cm^3, with uncertainties related to the profile of the galactic halo. The velocity distribution $\tilde{f}(\mathbf{v}, t)$ is a Maxwell-Boltzmann distribution boosted to the lab frame. This involves both the velocity $\mathbf{v}_\odot$ of the Sun with respect to the halo ($\simeq$ 220 km/s) and the velocity of the Earth $\mathbf{v}_\oplus$ with respect to the Sun. So we can perform a Galileian transformation and expand,

$$\tilde{f}(\mathbf{v}, t) = f(\mathbf{v} + \mathbf{v}_\odot + \mathbf{v}_\oplus) \simeq f(\mathbf{v} + \mathbf{v}_\odot) + \epsilon \cos \omega(t - t_0) \frac{\mathrm{d}f}{\mathrm{d}\epsilon}(\mathbf{v} + \mathbf{v}_\odot), \tag{1.34}$$

where ϵ is the ratio of the component of $\mathbf{v}_\oplus$ in the direction of $\mathbf{v}_\odot$ to the modulus $|\mathbf{v}_\odot|$, while $\omega = 2\pi/\text{year}$. This means that the interaction rate has a constant component as well as an *annual modulation*, a small but measurable signal. The final astrophysical property is $v_{\max}$, identified with the escape velocity, measured to be around 500 to 600 km/s [16].

Detector properties. Apart from the detector mass, which must be sized according to the desired event rate, the crucial quantity is $v_{\min}$. This can be related, through kinematical considerations concerning the DM-nucleus collision, to the threshold recoil energy E_{th} that the detector is capable of measuring, via

$$v_{\min} = \sqrt{\frac{m_N E_{\text{th}}}{2\mu^2}}, \qquad \mu = \frac{\mu_\chi \mu_N}{\mu_\chi + \mu_N}. \tag{1.35}$$

Cross section. The differential cross section can be obtained taking an effective operator approach. Consider a process like the one in section 1.3.3, this time with an intermediate scalar ϕ for an easy example. The low-energy ($q \ll m_\phi$) 4-fermion vertex corresponding to the UV-complete diagram

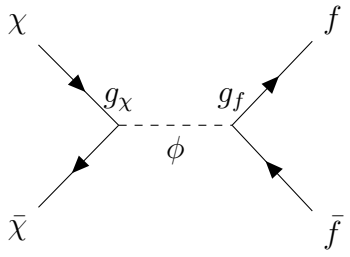

has a coupling strength $g_{\text{eff}} = g_\chi g_f / m_\phi^2$. In our case the SM particles will be quarks; since the scattering events are expected not to resolve the hadronic structure, though, we need to map quark fields Q onto nucleon fields p, n, by summing the couplings of χ with each quark flavour weighted over the fraction of the nucleon mass it accounts for. This way we obtain the coupling strengths of χ to protons f_p and neutrons f_n, which are usually the same. Then, we sum over all nucleons (Z protons and $A - Z$ neutrons) to obtain the matrix element for the DM-nucleus scattering process. Lorentz invariance of the matrix element and the Dirac equation restrict the ways the effective operator can depend on the momenta and lead to a scalar fermion bilinear for the nucleus $\overline{N}N$ multiplied by a

nuclear form factor $F(q)$, which can be modelled starting from experimental data. This means that the matrix element takes the form

$$\mathcal{M} = [Zf_p + (A-Z)f_n]\,\overline{\chi}\chi\overline{N}NF(q). \tag{1.36}$$

In the non-relativistic limit, $\overline{N}^s N^{s'} \simeq 2m_N \xi^{s\dagger}\xi^{s'}$, where the ξ are the numerical two-component spinors entering the free-particle solutions to Dirac equation, and an analogous expression holds for $\overline{\chi}\chi$. Summing over the spins and plugging the obtained non-relativistic matrix element squared into Fermi's golden rule, we obtain the *spin-independent* cross section:

$$\frac{\mathrm{d}\sigma}{\mathrm{d}E_\mathrm{R}} = \frac{2m_N}{\pi v^2}\left[Zf_p + (A-Z)f_n\right]^2 F^2(q). \tag{1.37}$$

If $f_p = f_n$, $\sigma \propto A^2$: the heavier the nucleus, the higher the cross section, and DM interacts coherently with the whole nucleus.
This is the simplest form of DM-nucleus scattering cross section. It is independent of the recoil energy, leaving the only dependence on E_R in (1.33) in the distribution function. Explicit dependence of the cross section on E_R can be obtained if the contribution of q to g_eff cannot be neglected, and/or if a more complicated χ bilinear enters the effective operator. The form of χ and N bilinears can also lead to *spin-dependent* interactions. Using e.g. $\mathcal{L}_\mathrm{eff} \propto \overline{\chi}\gamma_\mu\gamma^5\chi\,\overline{Q}\gamma^\mu\gamma^5 Q$, one gets

$$\frac{\mathrm{d}\sigma}{\mathrm{d}E_\mathrm{R}} = \frac{16m_N}{\pi v^2} G_\mathrm{F}^2 J(J+1)\Lambda^2 F_\mathrm{SD}^2(q), \tag{1.38}$$

where J is the nuclear spin, G_F the Fermi constant, $\Lambda \equiv \frac{1}{J}(f_p\langle S_p\rangle + f_n\langle S_n\rangle)$, and we have a different form factor.

Plugging typical numbers into (1.33) we get an integrated number of events of the order

$$\frac{R}{M_\mathrm{det}} \sim 0.13\,\frac{\mathrm{events}}{\mathrm{kg}\cdot\mathrm{year}}\left(\frac{A}{100}\right)\left(\frac{\sigma_0}{10^{-38}\,\mathrm{cm}^2}\right) \times \left(\frac{\langle v\rangle}{220\,\mathrm{km}\cdot\mathrm{s}^{-1}}\right)\left(\frac{\rho_0}{0.3\,\mathrm{GeV}\cdot\mathrm{cm}^{-3}}\right). \tag{1.39}$$

This relation can be used to estimate how big the detector should be and for how long the experiment should run. Upcoming detectors will reach tens and hundreds of tons in mass.
The signatures of nuclear recoils include heat, light and electrical currents due to electron displacements. Current experiments employ single- or two-phase noble gas tanks. One main difficulty, since nuclear recoils are extremely rare events, is the reduction of backgrounds, including natural radioactivity from the earth, cosmic rays, secondary particles and neutrinos.
Other searches involve the annual modulation. In particular, a variation in signal between June and December was observed by the DAMA experiment [17], but that result conflicts with subsequent experiments (e.g. [18]), sparking interest in models which tried to accommodate the discrepancy (see also section 3.1.1).

FIP/dark sector searches

The typical energy threshold for recoil experiments is a few keV. Then, according to equation (1.31), if m_χ gets lighter than the tens of GeV scale, E_R is below the threshold and one should really look for alternative methods. All these other possibilities involve many-body effects, and we list them below. Again, we will not focus on the details, for which the reader can consult [19].

Electron recoils. Electrons are much lighter than nucleons, and therefore move faster. Considering the electrons in a bound state with the nuclei, the single electron has a Compton wavelength of roughly one Bohr radius $R_\mathrm{Bohr} = 1/(\alpha m_e)$, which corresponds to a momentum $k_e \simeq \alpha m_e$ and a velocity $v_e \simeq \alpha$. The electron is in an energy eigenstate; to move to the momentum eigenstates requires the dispersion relation in the material, hence the many-body effects coming into play. We report an estimate for the scattering rate [19], with $\sigma_0 \simeq 10^{-37}$ cm^2, $m_\chi = 10$ MeV and $N_\mathrm{t} \simeq 10^{25}$:

$$\frac{R}{M_\mathrm{det}} \sim 50 - 100 \frac{\text{events}}{\text{kg} \cdot \text{day}}. \tag{1.40}$$

Compared to nuclear recoils, these numbers look extremely promising, but lower energy thresholds imply that controlling backgrounds is much more challenging. Existing experiments (e.g. XENON10/100 [20] and DarkSide [21]) have been shown to be sensitive to these searches.

Migdal effect. When a DM particle scatters off a nucleus, electrons will follow the recoiling nucleus with a lag. This causes ionisation and excitation of the surrounding medium which can be detected [22].

Scattering in a lattice. If m_χ is low enough, it can cause excitations in semiconductor targets provided it can clear the ~ 1 eV band gap [23].

Phonon couplings. Another effect of DM-nuclei interactions can be the collective displacement of the atoms in a lattice. This is particularly relevant for sub-MeV candidates, as the momentum transfer is so low that phonons are the relevant degrees of freedom [24].

1.4.2 Indirect detection

Indirect searches looks for DM annihilation products in astrophysical objects, where DM is expected to reach a sufficiently high density. The inner parts of the Galaxy are a particularly favourable environment for this to happen, and we can look, e.g., at neutral probes in the directions around the galactic center. Detailed discussion about indirect DM detection can be found in [25], [26], [27] and references therein.

WIMP searches

The kind of SM particle we can look for depends on the annihilation process itself. We can have either primary annihilation products, which are expected to be easier to detect as they exhibit spikes in their spectrum, or secondary ones, which have continuous spectra as they result from subsequent decays of the primary particles.

Photons. The production of photons from annihilation can proceed in three main ways, each with its own spectral signature: loop-level direct annihilation, final- or intermediate-state radiation, and meson decay from hadronisation. Sources include the galactic centre, dwarf galaxies, distant clusters and diffuse gamma-ray background.
The photon flux detectable by on-earth or satellite-bound telescopes is quantified as

$$\frac{\mathrm{d}N_\gamma}{\mathrm{d}E\,\mathrm{d}t\,\mathrm{d}A} = \frac{1}{4\pi}\,J\sum_i \frac{\langle\sigma_i v\rangle}{2m_\chi^2}\frac{\mathrm{d}N_i}{\mathrm{d}E_\gamma}. \tag{1.41}$$

This formula can be essentially divided in two parts.

- The J factor
$$J = \int_{\Delta\Omega}\mathrm{d}\Omega\int_{\text{l.o.s.}}\rho_\chi^2(\ell,\Omega)\,\mathrm{d}\ell, \tag{1.42}$$
contains all the astrophysical properties, namely the location of sources, the velocity distribution and the DM profile; ℓ is the distance along the line of sight (l.o.s.), $\Delta\Omega$ the angle subtended by the observed object (or the aperture of the telescope). The highest J factor is that of the galactic centre (up to $\sim 10^{25}$ GeV^2/cm^5), but stellar activity is a significant background; this can be contrasted with dwarf galaxies, which are dimmer but have lower J factors.

- The remaining factor depends on particle physics properties: we have a sum, over the annihilation channels, of the thermally averaged cross sections, divided by the mass of the DM particles, multiplied by the spectrum of the photons produced in the processes. A factor 1/2 accounts for the fact that in most models photons are produced in pairs.

Antimatter. Antiparticles are an excellent DM tracer, as they are not commonly produced in astrophysical processes. Experiments dedicated to cosmic ray detection, both on earth and on satellites, are usually capable of distinguishing antimatter. Besides antideuterium, which would be a clear DM activity signal as no known process is able to produce it, our attention goes to positron and antiproton excesses.
Positrons from DM annihilation can be either primary or secondary. They undergo substantial energy loss as they travel around the Galaxy, so the interesting sources are the closest ones ($\lesssim$ 100 pc). Famously, a positron excess was measured by PAMELA [28], and later confirmed by AMS-02 [29]. However, a probable explanation is emission from nearby pulsars [30].
AMS-02 also reported antiproton excesses [31], one of which is in the 10-20 GeV range and has no definitive astrophysical explanation. If interpreted as coming from DM annihilation, it was shown to fit very nicely with the relic density [32].

Neutrinos. Another promising DM annihilation probe is neutrinos. They can be produced in a variety of ways (direct production, hadronic decays and lepton decays) and a number of neutrino telescopes are in operation around the world. However, their cross sections are much smaller, giving weaker bounds with respect to other galactic and extragalactic probes.
A different source of neutrinos from DM annihilation is the Sun. If a WIMP interacts with a nucleus in the Sun, it can scatter at a velocity smaller than the escape velocity, remaining trapped. This way a DM overdensity can form, leading to efficient annihilation

processes inside the Sun, whose SM products either stay trapped (if charged), or escape. The latter is the case of neutrinos, which therefore constitute the possible signature of solar DM annihilation. The flux of neutrinos produced in this way,

$$\frac{\mathrm{d}\Phi}{\mathrm{d}E} = \frac{\Gamma_{\mathrm{ann}}}{4\pi R^2} \sum_i \mathrm{BR}_i \frac{\mathrm{d}N_i}{\mathrm{d}E}, \tag{1.43}$$

depends on the annihilation rate Γ_{ann} for the DM-nucleus interaction (analogous to the interaction rate for direct detection from section 1.4.1),[4] on the energy spectrum $\mathrm{d}N_i/\,\mathrm{d}E$ for each decay channel of the primary products, and on the earth to sun distance R. The more unstable the primary is, the higher the energy of the neutrinos it decays into will be; hard spectra are more constrained than weak ones, as their cross section is higher and backgrounds are lower. A comparison can be made with bounds from direct searches: while for spin-independent interactions solar WIMPs give weaker bounds than direct detection, for spin-dependent interactions the two are competing [33].

FIP/dark sector searches

In the sub-GeV mass range, the prime probes for DM annihilation are neutrinos, since their interactions are easily accommodated within dark sector models. The same considerations we made for WIMPs are valid here, especially for what concerns primary neutrino production $\chi\bar{\chi} \to \nu\bar{\nu}$. This is a 2-body process with a very clear signature, namely a narrow line at $E_\nu = m_\chi$.
If χ is a Majorana particle (see section 2.2) and we assume the same branching ratio for the three neutrino flavours, (1.41) yields, for one flavour,

$$\frac{\mathrm{d}\Phi}{\mathrm{d}E_\nu} \propto J \frac{1}{3} \frac{\langle\sigma v\rangle}{2} \delta(E_\nu - m_\chi). \tag{1.44}$$

Since we are dealing with sub-GeV neutrinos, the challenge in identifying DM annihilation events in the Sun is given by the backgrounds, which come from a variety of neutrino sources. This includes geoneutrinos, as well as reactor, atmospheric and supernova neutrinos. For those experiments that cannot distinguish neutrinos from antineutrinos, like water Cherenkov detectors, also solar neutrinos, invisible muon decays and muon-induced spallation products constitute backgrounds.

1.4.3 Collider and terrestrial searches

The class of searches we will review here is based on the aim of producing DM ourselves and observe its signature in appropriate detectors. Collider physics attempts to do so by smashing together accelerated SM particles (electron-positron pairs, reaching around 1 TeV in the center-of-mass frame, or hadrons, capping at 14 TeV at LHC) and then collecting the interaction products in multi-purpose detectors. The typical DM signatures we look for are missing energy and momentum in the direction transverse to the particle beam. A process whose only products are DM particles would leave no trace in the detectors. Instead, the collision may also produce a single gluon, resulting in a *monojet*

[4] Some care must be taken as, in the case at hand, the density ρ_χ is not simply given by the measured local DM density of 0.3 g/cm^3, but by the equilibrium density inside the sun, which takes into account the capture rate and annihilation rate on varying the density of the nuclei.

and missing energy, or a neutral gauge boson, resulting in a *monophoton* or *mono-Z* plus missing energy signature. Any competing process which produces neutrinos is a background, as neutrinos escape detection and results in missing energy as well. As we previously stated, no WIMPs have been produced this way, and this put tight bounds on SUSY models.
Moving to lower DM mass scales, an alternative to colliders is beam dump experiments. The setup slightly changes: an accelerated proton (or electron) beam is made to hit a dense target, producing mesons like $\pi^{\pm}$, π^0, $K^{\pm}, K^0$ and so on. The meson beam is focused via magnetic holes (if charged) and the products of the meson decays are then collected in detectors. While these experiments are suited for the observation of neutrino oscillations, they can also be used to probe dark sectors. Indeed, if enough energy is available, the decay of a neutral meson, say $\pi^0 \to \gamma\gamma$, may result instead in $\pi^0 \to \gamma Z'$, where Z' is a massive dark photon, mediating interactions in a secluded sector (more on that in the next chapters). The dark photon can then decay to a DM particle pair:

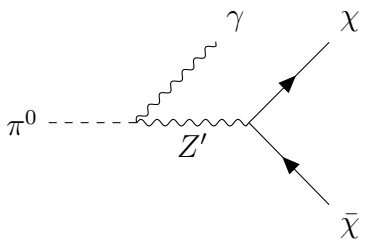

In the detector, the DM interacts very weakly with electrons or nucleons, through the same channels described in section 1.4.1. The recoils are difficult to tell apart from those related to neutrino-target interactions, so the neutrino flux from the other meson decays should always be suppressed, although this is unlikely to be the case in current fixed-target experiments, which are mainly dedicated to neutrino physics. Chapter 4 deals with a modified version of this setup, where a dark sector particle produced from Z' decay enters the detector and decays, in turn, to DM and a SM lepton pair; the leptons are then expected to leave a recognisable signature.

Chapter 2

Extending the Standard Model: dark sectors

The Standard Model of particle physics is one of the tremendous scientific conquests of the last century, consistently describing the quantum world together with the Lorentz invariance from special relativity. Its greatest confirmed predictions include the discovery of quarks, weak neutral currents, W and Z bosons, and the Higgs boson. Nonetheless, besides the obvious exclusion of gravity, the SM fails to account for a variety of phenomena currently at our empirical reach, among which the existence of neutrino masses stands out. We will review how this problem can be tackled in section 2.2.
This will prepare the ground for the introduction of Dark Sectors models, which add new particles that do not interact directly with the SM ones, but require some sort of 'messenger' particle to communicate. We will provide motivation for specific realisations of dark sectors, see how they address the shortcomings of the SM, and discuss their phenomenology.

2.1 A brief review of the Standard Model

Let us start by examining the mathematical structure of the SM, as found in textbooks like [34] and in the extensive Particle Data Group review [35]. Its formulation follows the guiding principle of symmetry in the Lagrangian formalism: a gauge group is introduced, together with a particle content, and the form of interaction terms follows from requiring the invariance of the Lagrangian under the gauge group. Mass terms are forbidden by the gauge symmetry itself, thus some mass generation mechanism must be included.

Gauge group

The internal, local symmetry group we consider is $SU(3)_C \times SU(2)_L \times U(1)_Y$. It is the product group of the gauge symmetries of quantum chromodynamics ($SU(3)_C$) and electroweak theory ($SU(2)_L \times U(1)_Y$). To make the kinetic term $i\overline{\psi}\gamma^\mu\partial_\mu\psi$ of a generic fermion ψ invariant under a gauge transformation we introduce the following covariant

derivatives:

$$SU(3)_C : D_\mu \equiv \partial_\mu + i\frac{g_s}{2}G^a_\mu \lambda^a, \tag{2.1}$$

$$SU(2)_L : D_\mu \equiv \partial_\mu + i\frac{g}{2}W^i_\mu \sigma^i, \tag{2.2}$$

$$U(1)_Y : D_\mu \equiv \partial_\mu + i\frac{g'}{2}Y B_\mu, \tag{2.3}$$

where λ^a denotes the eight Gell-Mann matrices, which generate $SU(3)$, and σ^i denotes the three Pauli matrices, which generate $SU(2)$. This defines the gluons G^a_μ, mediating the strong interaction with coupling g_s, and the gauge bosons W^i_μ and B_μ, that serve as the high-energy mediators for the unified electroweak interaction, with couplings g and g'. While the $SU(3)_C$ and $SU(2)_L$ coupling strengths are universal, the $U(1)_Y$ depends on the *weak hypercharge* Y of the specific fermion. Kinetic terms for the gauge bosons are added to the Lagrangian to describe their propagation:

$$\mathcal{L} \supset -\frac{1}{4}G^a_{\mu\nu}G^{\mu\nu}_a - \frac{1}{4}W^i_{\mu\nu}W^{\mu\nu}_i - \frac{1}{4}B_{\mu\nu}B^{\mu\nu}, \tag{2.4}$$

where the quantities with two Lorentz indices are the field strengths; for a gauge boson V^a_μ associated to a group whose structure constants are f^{abc}, and whose coupling is g_V, the field strength is defined as

$$F^a_{\mu\nu} \equiv \partial_\mu V^a_\nu - \partial_\nu V^a_\mu - g_V f^{abc} V_{\mu\, b} V_{\mu\, c}. \tag{2.5}$$

Barring the abelian $U(1)_Y$, these terms also include the cubic and quartic interactions among gauge bosons of the same subgroup.

Higgs mechanism

As anticipated, mass terms for the gauge bosons $m^2_V V^a_\mu V^\mu_a$ are manifestly incompatible with gauge invariance. However, we do need to introduce massive mediators for the electroweak sector to make contact with reality. Indeed, the UV completion of Fermi theory calls for a massive intermediate boson to open up the 4-fermion vertex and make sense of the low-energy observations of the weak interaction (e.g. muon decay). A viable solution involves spontaneous symmetry breaking (SSB), i.e. a scenario in which, while the Lagrangian (and therefore the underlying physical laws) stays gauge-invariant, the vacuum state of some specific field no longer respects the symmetry.
The field we are referring to, in the SM, is the scalar Higgs boson. We define it as the complex $SU(2)_L$ doublet

$$H = \begin{pmatrix} H^- \\ H^0 \end{pmatrix}. \tag{2.6}$$

The Lagrangian will then contain a Higgs sector, including a kinetic term, a mass term and a quartic self-interaction, all allowed by gauge invariance:

$$\mathcal{L} \supset (D_\mu H)^\dagger D_\mu H - \mu^2 H^\dagger H - \lambda (H^\dagger H)^2. \tag{2.7}$$

The first term contain the covariant derivative with respect to the electroweak gauge group (containing the terms from both (2.2) and (2.3)). The last two terms form the Higgs potential

$$V(H) = \mu^2 H^\dagger H + \lambda (H^\dagger H)^2. \tag{2.8}$$

Now, if $\mu^2 \geq 0$, the vacuum state, meaning the state for which $V(H)$ is minimum, is simply the null configuration $H = 0$. Expanding H around this minimum does not break any symmetry. If instead $\mu^2 < 0$, the origin of $\mathbb{C}^2$ becomes a maximum and the minimum points are on the sphere, centred at the origin, of radius $\sqrt{-\mu^2/2\lambda}$. We can choose, fixing the $SU(2)_L$ gauge to the so-called *unitary gauge*, to set the vacuum expectation value (*vev*) of the Higgs doublet to

$$\langle H \rangle = \begin{pmatrix} 0 \\ \frac{v}{\sqrt{2}} \end{pmatrix}, \qquad v \equiv \sqrt{\frac{-\mu^2}{\lambda}}, \tag{2.9}$$

and expand H in (2.7) around this value as

$$H = \frac{1}{\sqrt{2}} \begin{pmatrix} 0 \\ v + h(x) \end{pmatrix}. \tag{2.10}$$

This partially breaks $SU(2)_L \times U(1)_Y$, leaving a subgroup $U(1)_{\text{em}}$, the symmetry associated to electromagnetic interaction, unbroken. According to Goldstone's theorem, the theory must then possess three massless scalar bosons (Nambu-Goldstone bosons, or NGBs), one for each broken generator of the electroweak gauge group. By a suitable field redefinition, it can be shown that the NGBs come to form the longitudinal degrees of freedom of the weak interaction mediators $W_\mu^\pm$ and Z_μ, leaving the photon field A_μ transversal:

$$W_\mu^\pm = \frac{1}{\sqrt{2}} \left(W_\mu^1 \mp i W_\mu^2 \right), \tag{2.11}$$

$$Z_\mu = c_{\text{W}} W_\mu^3 - s_{\text{W}} B_\mu, \tag{2.12}$$

$$A_\mu = s_{\text{W}} W_\mu^3 + c_{\text{W}} B_\mu, \tag{2.13}$$

with c_{W} and s_{W} respectively denoting the cosine and sine of the Weinberg angle θ_{W}, derived from the couplings through the relations

$$\cos\theta_{\text{W}} = \frac{g}{\sqrt{g^2 + g'^2}}, \qquad \sin\theta_{\text{W}} = \frac{g'}{\sqrt{g^2 + g'^2}}. \tag{2.14}$$

Their masses, obtained again from the expansion of (2.7) around the Higgs *vev*, are given by

$$m_W = \frac{gv}{2}, \qquad m_Z = \frac{\sqrt{g^2 + g'^2}}{2}\, v, \qquad m_A = 0. \tag{2.15}$$

Particle content

We now discuss the elementary fermions in our model, which account for the known matter particles in our Universe. We have *quarks*, which couple to the full gauge group, and *leptons*, which couple only to the electroweak subgroup. Quarks and leptons can be classified as $SU(2)_L$ representations. A striking feature of the $SU(2)_L$ interaction is that it is chiral: left-handed fermions are a different representation (doublet) than right-handed fermions (singlet). Furthermore, we distinguish three generations of quarks and leptons, according to their interaction channels, providing the quantum numbers collectively known as *flavour*. The full particle content is:

$$\begin{gathered} Q_L^1 = \tbinom{u_L}{d_L}, u_R, d_R, \qquad Q_L^2 = \tbinom{c_L}{s_L}, c_R, s_R, \qquad Q_L^3 = \tbinom{t_L}{b_L}, t_R, b_R, \\ L_L^1 = \tbinom{\nu_e}{e}, e_R, \qquad L_L^2 = \tbinom{\nu_\mu}{\mu}, \mu_R, \qquad L_L^3 = \tbinom{\nu_\tau}{\tau}, \tau_R. \end{gathered} \tag{2.16}$$

Right-handed neutrinos are not included, since, as far as the SM is concerned, their lack of interactions (no weak interaction due to chirality and no electromagnetic interaction due to absence of charge) means they have never been detected.
Kinetic terms for all the fields in (2.16) are added to the Lagrangian, and, through covariant derivatives, their interactions with the gauge bosons are accounted for. Before electroweak SSB, the conserved currents associated to $SU(2)_L \times U(1)_Y$ are given by

$$J^i_\mu = \frac{1}{2}\overline{\psi_L}\gamma_\mu \sigma^i \psi_L, \qquad J^Y_\mu = 2\left(J^{\text{em}}_\mu - J^3_\mu\right), \tag{2.17}$$

where J^{em}_μ is the electromagnetic current. Upon SSB, these four currents mix, according to the field redefinitions in the previous subsubsection, giving rise to the physically observed interactions. The hypercharge Y and weak isospin T_3 are related to the electric charge Q of each fermion via the relation:

$$Q = T_3 + \frac{1}{2}Y. \tag{2.18}$$

Yukawa interactions

Just as for gauge bosons, mass terms for (Dirac) fermions are not allowed by gauge symmetry. Indeed, a mass term of the form

$$\mathcal{L}_{m,\,\text{Dir}} = -m\overline{\psi}\psi = -m\left(\overline{\psi_L}\psi_R + \overline{\psi_R}\psi_L\right) \tag{2.19}$$

contains products of $SU(2)_L$ doublets and singlets, thereby making the Lagrangian not invariant. Nonetheless, SSB can give masses to the fermions through Yukawa interactions with the Higgs. We write Yukawa terms for the up-type quarks, down-type quarks and charged leptons (neutrinos are considered massless at this stage):

$$\mathcal{L} \supset -y_u\overline{Q_L}\tilde{H}u_R - y_d\overline{Q_L}Hd_R - y_e\overline{L_L}He_R + \text{h.c.} \tag{2.20}$$

Here we define $\tilde{H} \equiv i\sigma^2 H^*$ to get the correct cancellation in hypercharge. When the Higgs gets a *vev*, as in (2.10), we get mass terms of the kind specified by (2.19), with $m = yv/\sqrt{2}$.
Now, expression (2.20) must be summed over generations (the y are 3×3 matrices), and an important consideration is to be made. We have defined our fields in (2.16) as eigenstates of the weak isospin, and separated them according to flavour; there is no reason why their mass eigenstates should perfectly align, and indeed they do not. We can set, by convention, the mass eigenstates of the up-type quarks (and of charged leptons) to their flavour eigenstates u, c, t (e, μ, τ). Then, the matrix y_d of Yukawa couplings is nondiagonal, and the mass basis is obtained by a unitary transformation in the d, s, b sector. The transformation matrix V_{CKM} is known as CKM matrix (Cabibbo, Kobayashi, Maskawa) and one can count its degrees of freedom[1] to be three angles and one phase,the latter responsible for CP violation in the weak sector.

[1]The independent parameters for a 3×3 unitary matrix are 3 angles and 6 phases; rotating the fields in a Dirac mass term by a $U(1)$ phase for each of the 6 quark flavours leaves the term invariant, so we subtract the 6 phases from the counting; but V_{CKM} is invariant if all the phases are the same, so we leave one free.

Further considerations

We are not interested in the QCD sector for this work in particular, but perhaps it is worth mentioning some of its features. The conserved charge for $SU(3)_C$ is *colour*. Quarks, of any flavour, belong to the fundamental representation **3** while gluons belong to the adjoint representation **8**. The strong interaction exhibits asymptotic freedom: it is weaker as the energy scale increases. This leads to having the perturbative regime at high energies, while, on the other hand, causes quarks and gluons to always form colourless bound states (*hadrons*) at low energies. The solution to the so-called *missing meson* problem, an issue related to the absence of a bound state predicted by an approximate axial $U(1)$ symmetry, led to the discovery of a CP-violating phase θ_{QCD} in the strong sector.
In addition to the gauge symmetry, the SM has global symmetries. Besides the Poincaré group, which is a fundamental symmetry for any relativistic field theory, there are four continuous global $U(1)$ symmetries that arise despite not being postulated in the formulation of the model. The conserved charges associated to these *accidental* symmetries are the baryon number B and the lepton family numbers $L_{e,\mu,\tau}$.
To end this section, we remark that the SM has 19 free parameters, to be selected among the quantities appearing throughout this section. The common choice is to prefer directly observable quantities over high-energy ones: the quark and charged lepton masses, the CKM matrix parameters, the gauge couplings, the strong CP phase, and the Higgs mass and *vev*.

2.2 Neutrino masses

Experiments such as SuperKamiokande [36] in 1998 and SNO [37] in 2001 proved the existence of *neutrino oscillations* beyond resonable doubt: neutrinos produced in a known flavour eigenstate can be detected, after travelling some distance, in a different flavour. This is explained by noticing that, in the vacuum, they propagate as eigenstates of the free particle Hamiltonian, which depends on their mass. The mass basis, just like for quarks, is not aligned with the flavour basis. Therefore, if the masses for the three neutrino flavours are not all the same, a mixing occurs during propagation, with a probability that depends on the difference between the square of the masses.
As we stated in section 2.1, the SM treats neutrinos as massless. One could think of simply introducing right-handed neutrinos ν_R, considered sterile under the SM gauge group, to write Dirac mass terms as in (2.19), and relate the mass eigenstates to the flavour eigenstates through a mixing matrix analogous to the CKM matrix, parametrised in terms of three angles θ_{12}, θ_{23}, θ_{13}, and a CP-violating phase δ. The mass terms could then be generated via Yukawa interaction terms with the Higgs like the ones in (2.20). This is not the end of the story, though, since, for uncharged fermions, we can also have Majorana mass terms:

$$\mathcal{L}_{m,\,\text{Maj}} = -\frac{1}{2} m \overline{\psi^c} \psi + \text{h.c.} = \frac{1}{2} m \psi^T C^\dagger \psi + \text{h.c.}, \tag{2.21}$$

where $C = i\gamma^0\gamma^2$ is the charge conjugation operator and $\psi^c = C\overline{\psi}^T$ is the charge-conjugated field. Indeed, whether neutrinos are Majorana or Dirac particles (i.e. the same as their antiparticle or not) has not been settled yet. This is an important question, since Majorana neutrinos would imply that lepton number is not a meaningful quantum

number: it is easily seen that (2.21) is not invariant under a $U(1)$ rephasing of the field. This has important consequences, for instance, in baryogenesis.
Let us see what this implies for the mixing matrix. Take the charged-current interaction term in the SM Lagrangian:

$$\mathcal{L} \supset -\frac{g}{\sqrt{2}} \sum_{\alpha=e,\mu,\tau} \overline{L_L^\alpha} \gamma^\mu W_\mu \nu_L^\alpha + \text{h.c.}. \tag{2.22}$$

If, as we did in section 2.1, we choose the charged lepton mass basis to correspond to the flavour basis, the neutrino mass basis should be related to the flavour basis through a unitary matrix. This time, if neutrinos are Majorana, rephasing the fields is not harmless, unless of course the three neutrinos are rotated with the same phase. This brings us to a total of two relative physical phases among the neutrinos entering as independent parameters in the mixing matrix. The resulting PMNS matrix (Pontecorvo, Maki, Nakagawa, Sakata) is of the form:

$$U_{\text{PMNS}} = \begin{pmatrix} 1 & 0 & 0 \\ 0 & c_{23} & -s_{23} \\ 0 & s_{23} & c_{23} \end{pmatrix} \begin{pmatrix} c_{13} & 0 & -s_{13}\mathrm{e}^{-i\delta} \\ 0 & 1 & 0 \\ s_{13}\mathrm{e}^{-i\delta} & 0 & c_{13} \end{pmatrix} \begin{pmatrix} c_{12} & s_{12} & 0 \\ -s_{12} & c_{12} & 0 \\ 0 & 0 & 1 \end{pmatrix} \times \begin{pmatrix} 1 & 0 & 0 \\ 0 & \mathrm{e}^{i\alpha_{21}/2} & 0 \\ 0 & 0 & \mathrm{e}^{i\alpha_{31}/2} \end{pmatrix}, \tag{2.23}$$

where c_{ij} and s_{ij} respectively denote the cosine and sine of the mixing angle θ_{ij} (this space-saving subscript notation for trigonometric functions will be adopted several times throughout this work), while α_{21} and α_{31} are the Majorana phases.
For each neutrino species we can write a Dirac mass term and two Majorana mass terms, one for the left-handed and one for the right-handed components:

$$\mathcal{L}_m = -m_D \overline{\nu_R} \nu_L - \frac{1}{2} \mu_L \overline{\nu_L^c} \nu_L - \frac{1}{2} \mu_R \overline{\nu_R^c} \nu_R + \text{h.c.} \tag{2.24}$$

or equivalently, after some algebra,

$$\mathcal{L}_m = -\frac{1}{2} \begin{pmatrix} \overline{\nu_L^c} & \overline{\nu_R} \end{pmatrix} \begin{pmatrix} \mu_L & m_D \\ m_D & \mu_R \end{pmatrix} \begin{pmatrix} \nu_L \\ \nu_R^c \end{pmatrix} + \text{h.c.} \tag{2.25}$$

The physical mass states are then obtained by diagonalising this mass matrix. In any case, if the Majorana masses μ_L and μ_R are nonvanishing, lepton number is not conserved and the neutrinos are Majorana.
Any mass term for neutrinos will break $SU(2)_L$, just like for other fermions. Thus we need a mass generation mechanism, which also accounts for the smallness of neutrino masses, which are most likely below the eV scale.[2] Introducing a Yukawa term, as in (2.20),

$$\mathcal{L} \supset -y_\nu \overline{L_L} \tilde{H} \nu_R + \text{h.c.} \tag{2.26}$$

we get a Dirac mass term from the Higgs getting a *vev*. However, this results in an extremely small Yukawa coupling $y_\nu = \sqrt{2} m_\nu / v \sim 10^{-12}$, which is unsatisfactory from

[2]KATRIN experiment [38] set $m_\nu < 0.8$ eV; cosmology gives even tighter bounds for the combined mass of the active species.

a naturalness perspective. If we give up lepton number as a fundamental symmetry, we can write Weinberg's dimension-5 operator, which is compatible with the SM gauge symmetry and gives rise to a Majorana mass term upon SSB:

$$-\frac{1}{2}\lambda\frac{\overline{L_L^c}\tilde{H}^*\tilde{H}^\dagger L_L}{\Lambda} \qquad \xrightarrow{\text{SSB}} \qquad -\frac{\lambda v^2}{2\Lambda}\nu_L^T C^\dagger \nu_L. \tag{2.27}$$

The UV completion of this model requires the $\nu\nu HH$ vertex to be opened up by inserting the propagator of a particle whose mass is $O(\Lambda)$. Depending on the Poincaré and $SU(2)_L$ representation of such particle, we get the different types of *seesaw* models.

Type I seesaw

The most studied seesaw model is type I, for which the intermediate particle is a heavy neutral lepton (HNL), basically a right-handed neutrino N_R whose mass is far greater than SM fermion masses. The terms added to the Lagrangian are

$$\mathcal{L} \supset y_\nu \overline{L_L}\tilde{H}N_R - \frac{1}{2}\overline{N_R^c}M_R N_R + \text{h.c.}. \tag{2.28}$$

Restricting to one generation, we get a Majorana term (only for N_R) and a Dirac term with mass $m_D = y_\nu v/\sqrt{2}$. Diagonalising the mass matrix

$$\mathfrak{M} = \begin{pmatrix} 0 & m_D \\ m_D & M_R \end{pmatrix} \tag{2.29}$$

we get the two eigenvalues

$$m = \frac{M_R \pm \sqrt{M_R^2 + 4m_D^2}}{2} \simeq \begin{cases} M_R & \text{(heavy state)} \\ -\frac{m_D^2}{M_R} & \text{(light state)} \end{cases} \tag{2.30}$$

for $m_D \ll M_R$. Adjusting M_R it is possible to get the light state mass m_ν to the experimental neutrino mass scale. When all three generations come into play, we have to diagonalise the full mass matrix, which has the form

$$\mathfrak{M} = \begin{pmatrix} 0_{3\times 3} & m_D \\ m_D^T & M \end{pmatrix}, \tag{2.31}$$

with M the (symmetric) heavy neutrino mass matrix. The seesaw formula (2.30) is generalised by

$$m_\nu = -m_D M^{-1} m_D^T + O((m_D M^{-1})^2) \tag{2.32}$$

for what concerns the light states. To see this, we can follow [39] and look at the generic unitary matrix Ω that makes $\mathfrak{M}$ block-diagonal, i.e.

$$\Omega^T \mathfrak{M} \Omega = \begin{pmatrix} m_\nu & 0_{3\times n} \\ 0_{n\times 3} & \tilde{M} \end{pmatrix}. \tag{2.33}$$

As with any unitary matrix, Ω can be formally written as the exponential of an antihermitian matrix:

$$\Omega = \exp\begin{pmatrix} 0_{3\times 3} & R \\ -R^\dagger & 0_{n\times n} \end{pmatrix} = \begin{pmatrix} \mathbb{1} - \frac{1}{2}RR^\dagger & R \\ -R^\dagger & \mathbb{1} - \frac{1}{2}R^\dagger R \end{pmatrix} + O(R^3). \tag{2.34}$$

With this expansion, (2.33) gives

$$m_D - R^* M \simeq 0, \tag{2.35}$$

$$-m_D R^\dagger - R^* m_D^T + R^* M R^\dagger \simeq m_\nu, \tag{2.36}$$

$$M + R^T m_D + m_D^T R \simeq \tilde{M}. \tag{2.37}$$

to leading order in R. From (2.35) we deduce that $R^* \simeq m_D M^{-1}$. Substituting into (2.36) and (2.37), we get the seesaw formula (2.32) and $\tilde{M} \simeq M$, completing the analogy to the one-generation case. The matrix m_ν we obtain is not diagonal in general, since we are still in the interaction basis, and can be diagonalised through the PMNS matrix (2.23).

Casas-Ibarra parametrisation

We now present a way of expressing the Yukawa matrix y_ν in terms of the physical masses, basically reversing equation (2.30), due to J. A. Casas and A. Ibarra [40]. If $\hat{m}_\nu$ and $\hat{M}^{-1}$ are the diagonalised counterparts of the light neutrino and inverse heavy neutrino mass matrices, we can write

$$\hat{m}_\nu = -U^T m_\nu U = -\frac{v^2}{2} U^T y_\nu \hat{M}^{-1} y_\nu^T U \tag{2.38}$$

(we dropped the subscript from the PMNS matrix, calling it simply U). Sandwiching this relation with $\sqrt{\hat{m}_\nu^{-1}}$ we obtain

$$\mathbb{1} = -\frac{v^2}{2} \sqrt{\hat{m}_\nu^{-1}}\, U^T y_\nu \hat{M}^{-1} y_\nu^T U \sqrt{\hat{m}_\nu^{-1}} \equiv \mathcal{O}^T \mathcal{O}. \tag{2.39}$$

The matrix

$$\mathcal{O} = \pm i \frac{v}{\sqrt{2}} \sqrt{\hat{M}^{-1}}\, y_\nu^T U \sqrt{\hat{m}_\nu^{-1}} \tag{2.40}$$

is therefore a complex orthogonal matrix (or semiorthogonal if rectangular). Inverting this definition, we get the Casas-Ibarra parametrisation of the Yukawa matrix:

$$y_\nu = \pm \frac{i\sqrt{2}}{v} U \sqrt{\hat{m}_\nu}\, \mathcal{O}^T \sqrt{\hat{M}}. \tag{2.41}$$

If U_M is the matrix that diagonalises M, that is

$$M = U_M^* \hat{M} U_M^\dagger, \tag{2.42}$$

we can write

$$y_\nu = \pm \frac{i\sqrt{2}}{v} U \sqrt{\hat{m}_\nu}\, \mathcal{O}^T \sqrt{M} U_M^\dagger. \tag{2.43}$$

2.3 Dark sectors and portal interactions

As stated in section 1.3.3, high-energy collider experiments produced no convincing result for physics at the TeV scale, leading to a growing interest in new degrees of freedom at the low-intensity frontier, in a mass range currently available to experiments (approximately

MeV to GeV). These particles constitute dark (or hidden) sectors, which can be thought of as either completely secluded (as described e.g. in [19]) or feebly communicating with the SM. Focusing on the latter case, interaction with the SM is realised through operators in the Lagrangian, known as *portals*, involving intermediate particles (*messengers*), with couplings that are highly suppressed with respect to g and g'. The philosophy of the portal framework is exploring a reachable parameter space without making important theory-driven assumptions about unifying principles. This does not exclude a later embedding of dark sectors into a theory with a broader scope. According to the Lorentz representation of the messenger, different kinds of portals can be included in BSM extensions. We will now review them in few words.

Vector portal. One of the most appealing messengers, particularly for light freeze-out DM, is the dark photon or dark Z, a massive, neutral vector boson associated to a gauged $U(1)_D$ symmetry. This field is usually made to communicate to the SM by means of a small mixing with the neutral SM gauge bosons in the kinetic term of the Lagrangian. The theoretical implications are reviewed in section 2.4 and in the next chapter. As for the dark photon phenomenology, kinetic mixing allows for Z' production in any process involving high-energy photons; collider and extracted beam experiments give bounds both for visible decays (like $Z' \to e^- e^+$) and invisible decays (such as $Z' \to \chi\bar{\chi}$, with a missing energy signature). The DM candidate can then be a fermion, charged under $U(1)_D$, with a mass not too far away from that of Z' to comply with cosmological bounds.

Scalar portal. A dark scalar or dark Higgs Φ, which is a singlet of the SM, may be introduced with quartic (and possibly cubic) interactions with the SM Higgs boson, mixing with it. While this already gives a communication channel, if Φ has a nontrivial vacuum, upon EW and dark symmetry breaking it may gain a small Yukawa interaction with the SM fermions, affecting their mass. This yields a generation-dependent coupling, different from the dark photon one. Important cosmological and astrophysical bounds exist for models involving dark scalars.

Neutrino portal. As we discussed in section 2.2, one can introduce right-handed neutrinos to account for neutrino masses. If the neutrino can "talk" to the dark sector through an operator, maybe involving a sterile neutrino and a dark scalar, we obtain a portal. This can lead to modifications of mass generation mechanisms for light neutrinos, as we will see in section 3.2. Neutrino portals are tested in heavy neutral lepton peak and decay searches.

Pseudoscalar portal. The only known non-renormalisable portal involves axions or axion-like particles (ALP) as messengers. The EFT Lagrangian couples the axion only to the gluons, but the UV completion may also couple it to SM fermions, as can happen for more generic pseudoscalars. Both are compatible with thermal freeze-out, with the ALP picture offering more flexibility. Lab searches are mostly model-independent, being only based on the couplings; astrophysical searches include *haloscopes* and *helioscopes*.

2.4 Minimal kinetic mixing model

To illustrate the workings of portals, we will now show the implications of extending the SM with a kinetically-mixed dark photon. Following e.g. [41], we augment the SM symmetry group by introducing a new abelian symmetry denoted as $U(1)_D$. Any particle charged under $U(1)_D$ will be called "dark". We define a covariant derivative for the subgroup $SU(2)_L \times U(1)_Y \times U(1)_D$,

$$D_\mu \equiv \partial_\mu - i\frac{g}{2}W_\mu^i\sigma_i - ig'YB_\mu - ig_DY_DX_\mu, \tag{2.44}$$

and write out the kinetic terms for the gauge fields, including a term inducing a small mixing between the fields B and X:[3]

$$\mathcal{L}_{\text{gauge}} = -\frac{1}{4}W^i_{\mu\nu}W_i^{\mu\nu} - \frac{1}{4}B_{\mu\nu}B^{\mu\nu} - \frac{1}{4}X_{\mu\nu}X^{\mu\nu} - \frac{\varepsilon}{2}B_{\mu\nu}X^{\mu\nu}. \tag{2.45}$$

The mixing term can be thought of as coming from a vacuum polarisation diagram in the UV-complete theory, with a loop of new heavy fermions coupled to both gauge fields, capable of turning one boson into another. From this consideration we get the typical value of ε to be around 10^{-3}. It can be helpful to set $\varepsilon \equiv \sin\chi$, so that

$$\sqrt{1-\varepsilon^2} = \cos\chi, \qquad \frac{\varepsilon}{\sqrt{1-\varepsilon^2}} = \tan\chi. \tag{2.46}$$

Transforming the B and X fields, according to the relation

$$\begin{pmatrix} B_\mu \\ X_\mu \end{pmatrix} = \begin{pmatrix} \frac{1}{\sqrt{1-\varepsilon^2}} & 0 \\ -\frac{\varepsilon}{\sqrt{1-\varepsilon^2}} & 1 \end{pmatrix} \begin{pmatrix} \tilde{B}_\mu \\ \tilde{X}_\mu \end{pmatrix} \tag{2.47}$$

we get the canonical kinetic Lagrangian:

$$\mathcal{L}_{\text{gauge}} = -\frac{1}{4}W^i_{\mu\nu}W_i^{\mu\nu} - \frac{1}{4}\tilde{B}_{\mu\nu}\tilde{B}^{\mu\nu} - \frac{1}{4}\tilde{X}_{\mu\nu}\tilde{X}^{\mu\nu}. \tag{2.48}$$

This operation lets us find the propagators of the low-energy degrees of freedom, transferring the effect of the kinetic mixing to the mass and interaction terms. In particular, off-diagonal mass terms are generated. We can, however, exploit the invariance of (2.48) under rotations to diagonalise the mass Lagrangian and get the propagating, physical degrees of freedom, as explained below.
We take (2.7) and expand it around the Higgs *vev*, obtaining the mass terms:

$$(D_\mu H)^\dagger D^\mu H \supset \frac{g^2v^2}{4}W_\mu^+W^{-\mu} + \frac{g^2v^2}{8}W_\mu^3W_3^\mu + \frac{g'^2v^2}{8}B_\mu B^\mu - \frac{gg'v^2}{4}W_\mu^3B^\mu, \tag{2.49}$$

where $W_\mu^\pm$ is given by (2.11). We then add a mass term $m_X^2X_\mu X^\mu/2$ for the X boson, with no hypothesis about its origin as of yet.[4] Focusing on the terms involving B, W_3 and X, we get (omitting Lorentz indices)

$$\mathcal{L}_{m,\text{gauge}} \supset \frac{1}{2}\begin{pmatrix} B & W_3 & X \end{pmatrix} \begin{pmatrix} \frac{g'^2v^2}{4} & -\frac{gg'v^2}{4} & 0 \\ -\frac{gg'v^2}{4} & \frac{g^2v^2}{4} & 0 \\ 0 & 0 & m_X^2 \end{pmatrix} \begin{pmatrix} B \\ W_3 \\ X \end{pmatrix}. \tag{2.50}$$

[3] Mixing X with W_i in this way would be impossible because $W^i_{\mu\nu}$ is not gauge-invariant by itself, being the field strength of a nonabelian gauge theory.

[4] Interaction with a dark scalar is often invoked. Another possibility is a Stückelberg mass.

Applying the transformation (2.47), which we write, using (2.46), as

$$\begin{pmatrix} B \\ W_3 \\ X \end{pmatrix} = E \begin{pmatrix} \tilde{B} \\ \tilde{W}_3 \\ \tilde{X} \end{pmatrix} \equiv \begin{pmatrix} c_\chi^{-1} & 0 & 0 \\ 0 & 1 & 0 \\ -t_\chi & 0 & 1 \end{pmatrix} \begin{pmatrix} \tilde{B} \\ \tilde{W}_3 \\ \tilde{X} \end{pmatrix}, \tag{2.51}$$

to (2.50), we get the mass Lagrangian in the new basis:

$$\mathcal{L}_{m,\,\text{gauge}} \supset \frac{(m_Z^{\text{SM}})^2}{2} \begin{pmatrix} \tilde{B} & \tilde{W}_3 & \tilde{X} \end{pmatrix} \begin{pmatrix} \frac{s_\text{W}+\mu^2 s_\chi^2}{c_\chi^2} & -\frac{s_\text{W} c_\text{W}}{c_\chi} & -\mu^2 t_\chi \\ -\frac{s_\text{W} c_\text{W}}{c_\chi} & c_\text{W}^2 & 0 \\ -\mu^2 t_\chi & 0 & \mu^2 \end{pmatrix} \begin{pmatrix} \tilde{B} \\ \tilde{W}_3 \\ \tilde{X} \end{pmatrix}. \tag{2.52}$$

Here, m_Z^{SM} is the SM value given by (2.15) and $\mu \equiv m_X / m_Z^{\text{SM}}$. Now we can proceed with the diagonalisation, and we do so by an orthogonal transformation given by the product of three rotations:

- first, we rotate by the angle χ in the $\tilde{B} - \tilde{X}$ plane;
- then, we do the usual Weinberg rotation as in (2.12) and (2.13), in the $\tilde{B} - \tilde{W}_3$ plane;
- finally, we rotate the obtained block-diagonal matrix

  $$\begin{pmatrix} 0 & 0 & 0 \\ 0 & 1 & s_\text{W} t_\chi \\ 0 & s_\text{W} t_\chi & \frac{\mu^2}{c_\chi^2} + s_\text{W}^2 t_\chi^2 \end{pmatrix}$$

  in the $\tilde{W}_3 - \tilde{X}$ plane by an angle β given by

  $$\tan 2\beta = \frac{2 s_\text{W}^2 t_\chi^2}{1 - \frac{\mu^2}{c_\chi^2} + s_\text{W}^2 t_\chi^2}. \tag{2.53}$$

This way we end up with a zero eigenvalue, which we identify with the photon mass, and with

$$m_Z^2 = (m_Z^{\text{SM}})^2 \left(1 + s_\text{W} t_\chi t_\beta\right), \qquad m_{Z'}^2 = (m_Z^{\text{SM}})^2 \left(1 - \frac{s_\text{W} t_\chi}{t_\beta}\right). \tag{2.54}$$

To summarise, we have moved from the original UV basis (B, W_3, X) to the low-energy basis (A, Z, Z'), according to the relation

$$\begin{pmatrix} B \\ W_3 \\ X \end{pmatrix} = E\, R(\chi) R(\theta_\text{W}) R(\beta) \begin{pmatrix} A \\ Z \\ Z' \end{pmatrix}. \tag{2.55}$$

This yields

$$\begin{cases} B = c_\text{W} A - (c_\beta s_\text{W} + s_\beta t_\chi) Z + (s_\beta s_\text{W} - c_\beta t_\chi) Z' \\ W = s_\text{W} + c_\beta c_\text{W} Z - s_\beta c_\text{W} Z' \\ X = \frac{s_\beta}{c_\chi^2} Z + \frac{c_\beta}{c_\chi^2} Z' \end{cases} \tag{2.56}$$

To write out the interaction terms, it is useful to express the SM states $(A^{\mathrm{SM}}, Z^{\mathrm{SM}})$ in terms of the new ones. To do so, we can simply apply $R(\theta_{\mathrm{W}})^{-1}$ to and obtain

$$\begin{cases} A^{\mathrm{SM}} = A - s_\beta c_{\mathrm{W}} t_\chi Z - c_\beta c_{\mathrm{W}} t_\chi Z' \\ Z^{\mathrm{SM}} = (c_\beta + s_\beta s_{\mathrm{W}} t_\chi) Z + (-s_\beta + c_\beta s_{\mathrm{W}} t_\chi) Z' \end{cases} \tag{2.57}$$

This way we can just substitute for the new degrees of freedom in the interaction Lagrangian:

$$\begin{aligned} \mathcal{L}_{\mathrm{int}} \supset\ & e A^{\mathrm{SM}}_\mu J^\mu_{\mathrm{em}} + \frac{g}{2c_{\mathrm{W}}} Z^{\mathrm{SM}}_\mu J^\mu_{\mathrm{NC}} + g_D X_\mu J^\mu_D = \\ & e A_\mu J^\mu_{\mathrm{em}} + \\ & Z_\mu \left[\left(\frac{c_\beta}{c_{\mathrm{W}}} + s_\beta t_{\mathrm{W}} t_\chi \right) \frac{g}{2} J^\mu_{\mathrm{NC}} + \frac{s_\beta}{c_\chi} g_D J^\mu_D \right] + \\ & Z'_\mu \left[-c_\beta c_{\mathrm{W}} t_\chi e J^\mu_{\mathrm{em}} + \left(-\frac{s_\beta}{c_{\mathrm{W}}} + c_\beta t_{\mathrm{W}} t_\chi \right) \frac{g}{2} J^\mu_{\mathrm{NC}} + \frac{c_\beta}{c_\chi} g_D J^\mu_D \right]. \end{aligned} \tag{2.58}$$

The angle β is controlled by the mass ratio μ of X to Z^{SM} through (2.53). Due to the smallness of ε, and therefore of χ, however, we can treat β in turn as small in any case. This means that the relevant terms in (2.58), for what concerns the communication between the SM and the hidden sector, are those that couple Z' to the electromagnetic and neutral currents (of which the dominant term is the electromagnetic one); on the other hand, while the dark current is in fact coupled to the Z boson, the coupling strength is suppressed by a s_β factor. To make things easier in the following we can redefine $\varepsilon \equiv c_\beta c_{\mathrm{W}} t_\chi$, so that the dominant portal to the dark sector is simply given by $-\varepsilon e Z'_\mu J^\mu_{\mathrm{em}}$.

Chapter 3

Rich dark sector models

This chapter draws heavily on the work of A. Abdullahi *et al.* [42]. Their collection of rich dark sector models is motivated by the current strong bounds on both visible and invisible dark photon decays, and by the historical significance of non-minimal fermion models in the results of experiments probing Dark Matter.
We will start by outlining how the models are built, subsequently adding heavy Weyl fermions and finding the mass spectrum and phenomenological parameters at each degree of complexity. To make contact with relevant earlier proposals for DM, which we will also touch upon, a dark C symmetry will be introduced among other hypotheses. Section 3.2 will be devoted to the mass generation mechanism of light neutrinos with minimal additions to the Lagrangian.
Finally, section 3.3 will deal with how well non-minimal dark sectors adapt to the DM problem, presenting the parameter range that better reproduces the measured DM abundance.

3.1 Semi-visible dark photon models

The minimal kinetic mixing model presented in section 2.4 can lead, for the dark photon, to *visible* decays through the SM currents J^μ_{em} and J^μ_{NC}, as well as *invisible* decays through the dark current J^μ_D, for which we have made no assumptions so far. A third possibility, which evades experimental constraints, is *semi-visible* decay, containing both SM charged particles and dark fermions in the final state. This can be achieved in DS models containing more than one generation of HNFs, with varying masses, which allows intermediate dark states between the parent Z' and the final visible states with missing energy.
We will be studying models with n fermions, entering a dark current of the kind

$$J^\mu_D = \sum_{i,j=1}^{n} \overline{\psi}_i \left(V_{ij}\gamma^\mu + A_{ij}\gamma^\mu\gamma^5\right)\psi_j, \tag{3.1}$$

where we separate the vector and axial-vector couplings to account for potentially chiral vertices. Non-renormalisable interactions can also be considered in principle. The dark photon is taken to be heavier than all HNFs, so that it cannot end up in the final states of HNF decays, which will all be three-body. Invisible HNF decays are also excluded.

3.1.1 Two HNFs and inelastic dark matter

Starting from the dark photon Lagrangian in section 2.4, we add two Weyl fermions χ_L, χ_R of opposite parity. We assign the respective $U(1)_D$ charges Q_L, Q_R as well as both Dirac and Majorana mass terms, obtaining the following terms:

$$\mathcal{L}_{\text{2HNF}} = \overline{\chi_L} i \left(\not{\partial} - i g_D Q_L \not{Z}'\right) \chi_L + \overline{\chi_R^c} i \left(\not{\partial} + i g_D Q_R \not{Z}'\right) \chi_R^c \\ - \frac{1}{2}\left[\begin{pmatrix} \overline{\chi_L^c} & \overline{\chi_R} \end{pmatrix} \begin{pmatrix} \mu_L & m_\chi \\ m_\chi & \mu_R \end{pmatrix} \begin{pmatrix} \chi_L \\ \chi_R^c \end{pmatrix} + \text{h.c.} \right]. \quad (3.2)$$

Majorana masses break $U(1)_D$, so we could assume they come from the *vev* of a (secluded) dark Higgs interacting with the HNFs. Allowing for a relative Majorana phase φ between the two fermions, the transformation that diagonalises the mass matrix M is given by

$$\hat{M} \equiv \begin{pmatrix} m_1 & 0 \\ 0 & m_2 \end{pmatrix} = U^T M U, \quad U = \begin{pmatrix} \cos\theta & -\sin\theta \\ \sin\theta & \cos\theta \end{pmatrix} \begin{pmatrix} \mathrm{e}^{i\varphi} & 0 \\ 0 & 1 \end{pmatrix}, \quad (3.3)$$

with

$$\tan 2\theta = -\frac{m_\chi}{\Delta\mu}, \qquad \Delta\mu \equiv \frac{\mu_R - \mu_L}{2}. \quad (3.4)$$

The masses obtained this way are

$$m_1 = \mathrm{e}^{2i\varphi}\left(\mu - \sqrt{m_\chi^2 + (\Delta\mu)^2}\right), \quad (3.5)$$

$$m_2 = \mu + \sqrt{m_\chi^2 + (\Delta\mu)^2}. \quad (3.6)$$

Now, the Lagrangian in (3.2) is written in terms of left-handed Weyl fermions. To construct the Majorana mass eigenstates of mass m_i, $i = 1, 2$, we take the eigenstates ψ_{iL} resulting from the rotation in (3.3) and define

$$\psi_i = \psi_{iL} + \psi_{iL}^c. \quad (3.7)$$

The dark current, written in terms of these states, assumes the form

$$J_D^\mu = \frac{Q_A - Q_V \cos 2\theta}{2} \overline{\psi_2} \gamma^\mu \gamma^5 \psi_2 + \frac{Q_A + Q_V \cos 2\theta}{2} \overline{\psi_1} \gamma^\mu \gamma^5 \psi_1 + \\ i Q_V \sin 2\theta \sin\varphi \, \overline{\psi_2} \gamma^\mu \psi_1 + Q_V \sin 2\theta \cos\varphi \, \overline{\psi_2} \gamma^\mu \gamma^5 \psi_1, \quad (3.8)$$

where $Q_V \equiv (Q_L + Q_R)/2$ and $Q_A \equiv (Q_L - Q_R)/2$.

C symmetry and mass spectrum

The Lagrangian (3.2) can be made invariant under charge conjugation. Such transformation acts on the quantised Weyl fermions as

$$\mathcal{C} \chi_L \mathcal{C}^\dagger = \eta_c \chi_R^c, \qquad \mathcal{C} \chi_R \mathcal{C}^\dagger = \eta_c \chi_L^c, \quad (3.9)$$

with η_c a phase factor that we can set to 1. Recalling that $\psi^c = C\overline{\psi}^T$, it is straightforward to see that the eigenbasis of the C operator, which acts on the solutions of the Dirac equation, is given by

$$\chi_+ = \frac{\chi_L + \chi_R^c}{\sqrt{2}}, \qquad \chi_- = \mathrm{e}^{i\varphi} \frac{\chi_L - \chi_R^c}{\sqrt{2}}. \quad (3.10)$$

The intrinsic C-parity of its eigenstates and of the dark photon can be fixed as

$$C(\chi_\pm) = \pm 1, \qquad C(Z'_\mu) = -1. \tag{3.11}$$

With this choices, $\mathcal{L}_{\text{2HNF}}$ is invariant under C provided that $Q_A = 0$ (which also ensures anomaly cancellation) in the limit $\Delta\mu \to 0$. Indeed, in the basis given in (3.10), we have

$$\begin{aligned}\mathcal{L}_{\text{2HNF}} = {} & \overline{\chi_+} i\partial\!\!\!/ \chi_+ + \overline{\chi_-} i\partial\!\!\!/ \chi_- \\ & + g_D Z'_\mu \left[\frac{Q_A}{2} \left(\overline{\chi_+}\gamma^\mu\gamma^5\chi_+ + \overline{\chi_-}\gamma^\mu\gamma^5\chi_- \right) + iQ_V \overline{\chi_+}\gamma^\mu\chi_- \right] \\ & - \left[\frac{1}{2} \begin{pmatrix} \overline{\chi_-^c} & \overline{\chi_+^c} \end{pmatrix} \begin{pmatrix} \mathrm{e}^{-2i\varphi}(\mu - m_\chi) & -\mathrm{e}^{-i\varphi}\Delta\mu \\ -\mathrm{e}^{-i\varphi}\Delta\mu & \mu + m_\chi \end{pmatrix} \begin{pmatrix} \chi_- \\ \chi_+ \end{pmatrix} + \text{h.c.} \right]\end{aligned} \tag{3.12}$$

and we can immediately see that the mass matrix is diagonal in the C-symmetric limit, as if, in performing the transformation (3.10), we had already acted with U, with maximal mixing ($\theta \to \pi/4$, via (3.4)). Then, if we choose $\varphi = \pi/2$, we get

$$m_1 = m_\chi - \mu, \qquad m_2 = m_\chi + \mu. \tag{3.13}$$

Both mass terms are positive for $m_\chi > \mu$. The two eigenstates $\chi_\pm$ can be thought of as a pseudo-Dirac pair with a mass splitting equal to 2μ.
On a side note, the C-parity assignment (3.11) for the dark photon makes it so that the kinetic mixing term $\propto F_{\mu\nu}X^{\mu\nu}$ is not invariant under C, unless we identify this "dark" C with the SM charge conjugation, causing it to act nontrivially on both the SM and the dark sector.

Benchmarks 1 — iDM

Inelastic Dark Matter (iDM for short) was first theorised [43] as a way of reconciling the results of experiments DAMA and CDMS, the former compatible with the effect of a standard WIMP, the latter disproving it completely. The main difference between the two experiments was the target nuclei: DAMA used NaI (heavier) targets, while CDMS employed Ge (lighter) targets. The proposed solution had to produce different behaviours on varying the nucleus mass.
The aim of iDM models is therefore to negate the possibility of elastic scattering of DM halo particles off lighter nuclei. The simplest realisation is obtained with two states $\chi_\pm$, with $m_{\chi_-} < m_{\chi_+}$, such that only χ_+ can interact with the targets. If χ_- is the DM candidate, then it can scatter only by transitioning to χ_+. The threshold velocity for this to happen can be shown to depend on the nuclear mass: the lighter the nuclei, the stronger the constraint.
If we impose, in the two-HNF model at hand, that $Q_A = 0$, $\Delta\mu \to 0$ (and, for simplicity, $Q_V = 1$), we immediately see that the dark current (3.8) becomes completely off-diagonal, reducing to just

$$J^\mu_{\text{iDM}} = i\overline{\psi_2}\gamma^\mu\psi_1 + \text{h.c.} \tag{3.14}$$

The heavier state χ_+ acts as a coannihilator in the early universe to keep χ_- particles in the thermal bath, and allows the upscattering of χ_- off targets above the nuclear mass threshold. This way we get a basic iDM model, depending on the parameters m_1, $\Delta_{21} = (m_2 - m_1)/m_1$, $r = m_1/m_{Z'}$, α_D and ε. This simple explanation for the DAMA puzzle has been ruled out by direct detection experiments [44].

3.1.2 Three HNFs and mixed-iDM

If we add one completely sterile Weyl fermion η_L to the two-HNF Lagrangian, we obtain

$$\mathcal{L}_{\text{3HNF}} = \mathcal{L}_{\text{2HNF}} + \overline{\eta_L} i\partial\!\!\!/ \eta_L - \left[\frac{\mu'_L}{2}\overline{\eta_L^c}\eta_L + \Lambda_L \overline{\eta_L^c}\chi_L + \Lambda_R \overline{\eta_L^c}\chi_R^c + \text{h.c.}\right]. \tag{3.15}$$

From here, we can choose to impose the C symmetry for the dark HNFs χ_L, χ_R, or leave the Lagrangian as it is. In the former case, depending on the mass gaps, we can get either an iDM variant where the heavier state is a pseudo-Dirac pair (mixed-iDM, BP2) or a hierarchical spectrum with definite C-parities (BP4). In the latter case, we get a hierarchical spectrum with mixed C-parities (BP5). In both scenarios we have to renounce C conservation for the sterile state, due to the odd number of Weyl fermions.

C symmetry and mass spectrum

Moving to the (η_L, χ_-, χ_+) basis, with χ_-, χ_+ given by (3.10), we get the mass matrix

$$M = \begin{pmatrix} \mu'_L & -\mathrm{e}^{-i\varphi}\Delta\Lambda & \Lambda \\ -\mathrm{e}^{-i\varphi}\Delta\Lambda & -\mathrm{e}^{-2i\varphi}(\mu - m_\chi) & -\mathrm{e}^{-i\varphi}\Delta\mu \\ \Lambda & -\mathrm{e}^{-i\varphi}\Delta\mu & \mu + m_\chi \end{pmatrix}, \tag{3.16}$$

where $\Lambda \equiv (\Lambda_L + \Lambda_R)/\sqrt{2}$ and $\Delta\Lambda \equiv (\Lambda_R - \Lambda_L)/\sqrt{2}$. C conservation for the dark pair is obtained in the limit where both $\Delta\mu \to 0$ and $\Delta\Lambda \to 0$. Assigning positive C-parity to η_L, we can rotate by an angle α in the C-even eigenspace (from χ_+ to η_L) to diagonalise the mass matrix. The angle is given by

$$\tan 2\alpha = \frac{\Lambda}{m}, \qquad m \equiv m_\chi + \mu - \mu'_L. \tag{3.17}$$

The mass eigenstates are

$$\psi_1 = c_\alpha \eta_L + s_\alpha \chi_+, \qquad m_1 = \mu'_L - m\frac{\sin^2\alpha}{\cos 2\alpha}; \tag{3.18}$$

$$\psi_2 = \chi_-, \qquad m_2 = m_\chi - \mu; \tag{3.19}$$

$$\psi_3 = -s_\alpha \eta_L + c_\alpha \chi_+, \qquad m_3 = \mu'_L + m\frac{\cos^2\alpha}{\cos 2\alpha}; \tag{3.20}$$

where we set $\varphi = \pi/2$ to flip the sign of the mass of the C-odd state as we did in the two-HNF case. Next, we check what happens to the dark current in the C-symmetric limit. If we proceed with the construction of Majorana fields as in (3.7), set $Q_V = 1$, $Q_A = 0$, and choose the remaining Majorana phase in such a way that the interaction terms are real, we get

$$J^\mu_{\text{3HNF}} = \sin\alpha\, \overline{\psi_2}\gamma^\mu\psi_1 + \cos\alpha\, \overline{\psi_2}\gamma^\mu\psi_3 + \text{h.c.} \tag{3.21}$$

The current is fully off-diagonal, thanks to η not being coupled to the dark photon, and to the $\chi_\pm$ interactions themselves being off-diagonal, as we saw from (3.12) in the $\Delta\mu \to 0$ limit.

Benchmarks 2 — mixed-iDM

In the limit $\tan 2\alpha \ll 1$, i.e. $\Lambda/m \ll 1$, the splittings in the model are

$$m_3 - m_1 \simeq m + \frac{2\Lambda^2}{m}, \tag{3.22}$$

$$m_3 - m_2 \simeq \frac{\Lambda^2}{m} + 2\mu. \tag{3.23}$$

Taking μ small enough, we can treat ψ_2 and ψ_3 as forming a pseudo-Dirac fermion Ψ_2, provided coherence between the two is kept long enough. In this case, the mostly-sterile Majorana state ψ_1 can be treated as a DM candidate, while Ψ_2 acts as the coannihilator, recovering an iDM model. The dark current is given by

$$J^\mu_{\text{mixed}-\text{iDM}} = \sin\alpha\, \overline{\Psi_2}\gamma^\mu\psi_1 + \cos\alpha\, \overline{\Psi_2}\gamma^\mu\Psi_2 + \text{h.c.}. \tag{3.24}$$

If we express the masses in (3.18)–(3.20) in terms of the paramenters $\tan 2\alpha$ and $\Delta_{21} \equiv (m_2 - m_1)/m_1$, and expand up to $O(\tan^2 2\alpha)$, we get

$$m_1 \simeq \mu'_L - \frac{1}{4}\left(\Delta_{21}\mu'_L + 2\mu\right)\tan^2 2\alpha, \tag{3.25}$$

$$m_2 \simeq \mu'_L\left(1+\Delta_{21}\right) - \frac{1}{4}\left(1+\Delta_{21}\right)\left(\Delta_{21}\mu'_L + 2\mu\right)\tan^2 2\alpha, \tag{3.26}$$

$$m_3 \simeq \mu'_L\left(1+\Delta_{21}\right) + 2\mu - \frac{1}{4}\Delta_{21}\left(\Delta_{21}\mu'_L + 2\mu\right)\tan^2 2\alpha. \tag{3.27}$$

Such expressions can be further simplified by taking $\mu \to 0$, which amounts to choosing opposite (or vanishing) Majorana terms for χ_L and χ_R:

$$m_1 \simeq \mu'_L\left(1 - \frac{1}{4}\Delta_{21}\tan^2 2\alpha\right), \tag{3.28}$$

$$m_2 \simeq \mu'_L\left(1 - \frac{1}{4}\Delta_{21}\tan^2 2\alpha\right)\left(1+\Delta_{21}\right), \tag{3.29}$$

$$m_3 \simeq \mu'_L\left(1 - \frac{1}{4}\frac{\Delta_{21}}{1+\Delta_{21}}\tan^2 2\alpha\right)\left(1+\Delta_{21}\right). \tag{3.30}$$

This way, the mass splitting $\Delta_{32} \equiv (m_3 - m_2)/m_2$ between ψ_2 and ψ_3 is suppressed with respect to Δ_{21}:

$$\Delta_{32} \simeq \frac{1}{4}\frac{\Delta_{21}}{\left(1+\Delta_{21}\right)}\tan^2 2\alpha. \tag{3.31}$$

Benchmarks 4 — three Majorana fermions with dark C symmetry

For sizeable mixings, we get a model with a triple of Majorana fermions, which can be employed as HNLs to generate neutrino masses through seesaw mechanism [45]. The limit $\tan 2\alpha \gg 1$ provides a mild hierarchical spectrum with the asymptotic behaviour:

$$m_1 \simeq \mu'_L - \Lambda = \frac{1}{1+\Delta_{21}}\left(\mu'_L - 2\mu\right), \tag{3.32}$$

$$m_2 \simeq \mu'_L - 2\mu, \tag{3.33}$$

$$m_3 \simeq \mu'_L + \Lambda = \left(1 + \frac{\Delta_{21}}{1+\Delta_{21}}\right)\mu'_L + \frac{\mu}{1+\Delta_{21}}. \tag{3.34}$$

Sending $\mu \to 0$ as we did for BP2, we get

$$\Delta_{32} \simeq \frac{\Delta_{21}}{\left(1+\Delta_{21}\right)}. \tag{3.35}$$

Benchmark 5 — three Majorana fermions

If we do not impose C conservation, the eigenvalues of the mass matrix become quite involved as they are the solution to a complete cubic equation. A more pronounced hierarchy can be produced by tweaking the parameters. The dark current keeps the diagonal terms, so fully invisible decays are possible if no further assumptions are made. Again, the model can be used to generate neutrino masses.

3.1.3 Four HNFs and inelastic Dirac DM

Adding another sterile state η_R to the Lagrangian in (3.15), we obtain

$$\begin{aligned}\mathcal{L}_{\text{4HNF}} = \mathcal{L}_{\text{2HNF}} + \overline{\eta_L} i\partial\!\!\!/ \eta_L + \overline{\eta_R^c} i\partial\!\!\!/ \eta_R^c - \\ \left[\frac{1}{2} m_\eta \overline{\eta_L} \eta_R^c + \frac{1}{2} m_\eta \overline{\eta_R^c} \eta_L + \frac{\mu'_R}{2} \overline{\eta_R} \eta_R^c + \Lambda'_L \overline{\eta_R} \chi_L + \Lambda'_R \overline{\eta_R^c} \chi_R^c \right. \\ \left. + \frac{\mu'_L}{2} \overline{\eta_L^c} \eta_L + \Lambda_L \overline{\eta_L^c} \chi_L + \Lambda_R \overline{\eta_L^c} \chi_R^c + \text{h.c.} \right]. \quad (3.36)\end{aligned}$$

In this case, we have two families of HNF: dark (χ, charged under $U(1)_D$) and sterile (η, completely uncharged).

C symmetry and mass spectrum

Acting with C on (3.36), using (3.9), we immediately see that requiring C-symmetry entails that $\Lambda_L = \Lambda'_R$, $\Lambda'_L = \Lambda_R$. Defining the C-parity eigenstates $\eta_\pm$ in the sterile sector as we did for $\chi_\pm$, we move to the (η_-, η_+, χ_-, χ_+) basis. In the C-symmetric limit we get the following mass matrix:

$$M = \begin{pmatrix} m_\eta - \mu' & 0 & \Lambda_- & 0 \\ 0 & m_\eta + \mu' & 0 & \Lambda_+ \\ \Lambda_- & 0 & m_\chi - \mu & 0 \\ 0 & \Lambda_+ & 0 & m_\chi + \mu \end{pmatrix}, \quad (3.37)$$

where

$$\mu' \equiv \frac{\mu_R - \mu_L}{2}, \quad \Lambda_\pm \equiv \frac{\Lambda'_L + \Lambda_R}{2} \pm \frac{\Lambda_L + \Lambda'_R}{2} \to \Lambda_R \pm \Lambda_L. \quad (3.38)$$

The sign for the C-odd states gets flipped due to the choice of Majorana phases as usual. As expected, the C-even and C-odd sectors decouple. To diagonalise we perform two independent rotations, one for each C-parity eigenspace, by angles $\beta_\pm$ given by

$$\tan 2\beta_\pm = \pm \frac{2\Lambda_\pm}{\Delta_\pm}, \qquad \Delta_\pm = \pm (m_\chi - m_\eta) + \mu - \mu'. \quad (3.39)$$

The mass spectrum is then given by

$$\psi_1 = c_{\beta_-}\eta_- + s_{\beta_-}\chi_-, \qquad m_1 = m_\eta - \mu' + \Delta_- \frac{\sin^2\beta_-}{\cos 2\beta_-}; \tag{3.40}$$

$$\psi_2 = c_{\beta_+}\eta_+ + s_{\beta_+}\chi_+, \qquad m_2 = m_\eta + \mu' - \Delta_+ \frac{\sin^2\beta_-}{\cos 2\beta_-}; \tag{3.41}$$

$$\psi_3 = -s_{\beta_-}\eta_- + c_{\beta_-}\chi_-, \qquad m_3 = m_\chi - \mu - \Delta_- \frac{\sin^2\beta_-}{\cos 2\beta_-}; \tag{3.42}$$

$$\psi_4 = -s_{\beta_+}\eta_+ + c_{\beta_+}\chi_+. \qquad m_4 = m_\chi + \mu - \Delta_+ \frac{\sin^2\beta_-}{\cos 2\beta_-}. \tag{3.43}$$

With the usual choices for dark charges, the dark current takes the form

$$J^\mu_{\text{4HNF}} = c_{\beta_+}c_{\beta_-}\psi_4\gamma^\mu\psi_3 + s_{\beta_+}c_{\beta_-}\psi_4\gamma^\mu\psi_1 + s_{\beta_-}c_{\beta_+}\psi_3\gamma^\mu\psi_2 + s_{\beta_+}s_{\beta_-}\psi_2\gamma^\mu\psi_1 + \text{h.c.} \tag{3.44}$$

If μ, μ' and $\Lambda_\pm$ are sufficiently small with respect to m_χ and m_η, we obtain two pseudo-Dirac particles.

Benchmark 3 — i2DM

If we set $\mu = \mu' = 0$, and therefore $\Delta_+ = -\Delta_- \equiv \Delta$, for small values of $\beta_\pm$, the mass splittings behave as follows:

$$m_4 - m_3 \sim m_2 - m_1 \sim \Delta\left(\beta_+^2 - \beta_-^2\right). \tag{3.45}$$

If also $\beta_+ = \beta_- \equiv \beta$, which is equivalent to $\Lambda_+ = \pm\Lambda_-$, we recover an exact Dirac pair. This final model is known as inelastic Dirac dark matter [46] and works the same as iDM, but with Dirac fermions Ψ_1 (from the sum of ψ_1 and ψ_2, the mostly sterile DM candidate) and Ψ_2 (from ψ_3 and ψ_4, the mostly dark coannihilator) in place of Majorana. In terms of these combinations, the dark current becomes

$$J^\mu_{\text{i2DM}} = s_\beta^2\overline{\Psi_1}\gamma^\mu\Psi_1 + s_\beta c_\beta\left(\overline{\Psi_2}\gamma^\mu\Psi_1 + \text{h.c.}\right) + c_\beta^2\overline{\Psi_2}\gamma^\mu\Psi_2. \tag{3.46}$$

3.2 Light neutrino mass generation

The HNFs introduced in the previous section can be given Yukawa interaction terms with the SM neutrinos. This makes the HNFs unstable and therefore unsuited as DM candidates, but gives us the opportunity to establish a seesaw mechanism and generate mass terms for light neutrinos, as explained in section 2.2. Conversely, one can choose to forbid the Yukawa terms, e.g. postulating a Z_2 symmetry for all the DS fermions (which in turn can be attributed to the conservation of lepton number [47]), and propose the HNF as DM particles. The flexibility of the model lets us do either or both.

Rank of the mass matrix

Let us take a preliminary look at what happens in the different scenarios by inspecting the full mass matrix, which has the general form we presented in section 2.2:

$$\mathfrak{M} = \begin{pmatrix} 0_{3\times 3} & m_D \\ m_D^T & M \end{pmatrix}. \tag{3.47}$$

Recall that m_D denotes the Dirac mass matrix resulting from Yukawa terms when the scalars of the theory get a *vev*, and M is the $n \times n$ mass matrix for the n HNF (this time we are not assuming M to be diagonal from the start, even though it will not matter in the end). Depending on which elements of M and m_D are nonvanishing, we get different models recurring in the literature. As we are about to show, for what concerns the light neutrino mass generation, it is more convenient to have a nonvanishing Majorana mass term for the HNF that lack Yukawa interactions with the light states. Indeed, this increases the rank of the matrix allowing for more nonzero eigenvalues. This is best exemplified by comparing an Inverted Seesaw-like (ISS) scenario, which assigns in fact a nonzero Majorana mass μ for the stable HNF, against an Extended Seesaw-like (ESS) scenario, which does not. The ISS result is the same as the general and C-conserving models from the previous section.
For $n = 2$ we get (crosses denote nonzero Yukawa terms):[1]

$$\mathfrak{M}_{\text{ISS}} = \begin{pmatrix} 0 & 0 & 0 & 0 & \times \\ 0 & 0 & 0 & 0 & \times \\ 0 & 0 & 0 & 0 & \times \\ 0 & 0 & 0 & \mu & \Lambda \\ \times & \times & \times & \Lambda & 0 \end{pmatrix} \quad \mathfrak{M}_{\text{ESS}} = \begin{pmatrix} 0 & 0 & 0 & 0 & \times \\ 0 & 0 & 0 & 0 & \times \\ 0 & 0 & 0 & 0 & \times \\ 0 & 0 & 0 & 0 & \Lambda \\ \times & \times & \times & \Lambda & M_R \end{pmatrix} \tag{3.48}$$

By inspection, $\text{rank}(\mathfrak{M}_{\text{ISS}}) = 3$, so the zero eigenvalue of $\mathfrak{M}_{\text{ISS}}$ has algebraic multiplicity $m_a(0) = 2$ and the seesaw mechanism gives mass to only one light neutrino (in addition to the heavy ones). On the other hand $\text{rank}(\mathfrak{M}_{\text{ESS}}) = 2$, so $m_a(0) = 3$ and the model is incapable of accounting for light neutrino masses.
We have a more promising situation for $n = 3$:

$$\mathfrak{M}_{\text{ISS}} = \begin{pmatrix} 0 & 0 & 0 & 0 & \times & \times \\ 0 & 0 & 0 & 0 & \times & \times \\ 0 & 0 & 0 & 0 & \times & \times \\ 0 & 0 & 0 & \mu & \Lambda_1 & \Lambda_2 \\ \times & \times & \times & \Lambda_1 & 0 & 0 \\ \times & \times & \times & \Lambda_2 & 0 & 0 \end{pmatrix} \quad \mathfrak{M}_{\text{ESS}} = \begin{pmatrix} 0 & 0 & 0 & 0 & \times & \times \\ 0 & 0 & 0 & 0 & \times & \times \\ 0 & 0 & 0 & 0 & \times & \times \\ 0 & 0 & 0 & 0 & \Lambda_1 & \Lambda_2 \\ \times & \times & \times & \Lambda_1 & M_{R1} & 0 \\ \times & \times & \times & \Lambda_2 & 0 & M_{R2} \end{pmatrix} \tag{3.49}$$

Here, assuming that the nonzero Yukawa couplings form a submatrix of maximum rank, we have $\text{rank}(\mathfrak{M}_{\text{ISS}}) = 5$ and the seesaw gives mass to two of the light neutrinos. It is then possible to compare the obtained masses with the experimental values of the mass-squared differences, with the aim of reconstructing the Yukawa structure through a bottom-up approach. This is not possible in the ESS-like case, since $\text{rank}(\mathfrak{M}_{\text{ESS}}) = 4$ and two light neutrinos stay massless.
The $n = 4$ case is analogous for the ISS-like models, while for the ESS-like models the

[1] Notice that the order of the HNF entries is inverted ("sterile" first and "dark" last) with respect to the usual order found in literature, to make the rank of the matrices more readable.

rank is even lower, as we add another HNL with no Majorana term, ending up again with no mass for the light neutrinos.
In all cases, the terms on the diagonal of the heavy neutrino submatrix M are decisive, so in the following we will assume M to be diagonal, and define the Yukawa couplings in the hybrid basis (ν_α, ψ_i), where $\alpha = e, \mu, \tau$ is the weak flavour index for the SM neutrinos and $i = 1, \ldots, n$ is the mass eigenstate index for the HNFs.
Of course, if we forgo the aim of also providing a DM candidate, the Yukawa submatrix can have all nonzero entries, increasing the rank of $\mathfrak{M}$ to the point where it is always possible to give mass to two or three of the SM neutrinos.

Yukawa structure

To reconstruct natural Yukawa couplings for our models, we will use Casas-Ibarra formula (2.41), whose factors can be organised as follows:

- measured parameters, i.e. the PMNS matrix U and the square root of the light neutrino mass matrix $\hat{m}_\nu$, whose entries we take from [48] (assuming normal ordering, with the lightest neutrino being massless), and the Higgs *vev* $v = 246$ GeV;
- the arbitrary semiorthogonal matrix $\mathcal{O}^T$, which we parametrise in terms of complex angles;
- the square root of the HNF mass matrix $\hat{M}$, with m_{ψ_1} chosen in the MeV to GeV range and heavier states roughly one order of magnitude above that.

As we have seen above, the $n = 2$ case does not allow for the simultaneous generation of light neutrino masses and the presence of a DM candidate. The most general 3×2 complex semiorthogonal matrix can be parametrised as

$$\mathcal{O} = \begin{pmatrix} 0 & \cos\omega & \xi \sin\omega \\ 0 & -\sin\omega & \xi \cos\omega \end{pmatrix}, \tag{3.50}$$

where $\xi = \pm 1$ and $\omega = a + ib$ is a complex angle. If we turn off the rotational component by sending $a \to 0$, and consider the asymptotic behaviour for $b \gg 1$, we get

$$\mathcal{O} \sim \begin{pmatrix} 0 & 1 & i\xi \\ 0 & -i & \xi \end{pmatrix} \frac{\mathrm{e}^b}{2}. \tag{3.51}$$

For the considered mass range, we get

$$|y_\nu| \sim \begin{pmatrix} 10^{-10} - 10^{-8} & 10^{-10} - 10^{-9} \\ 10^{-10} - 10^{-8} & 10^{-10} - 10^{-8} \\ 10^{-10} - 10^{-8} & 10^{-10} - 10^{-8} \end{pmatrix} \frac{\mathrm{e}^b}{2}. \tag{3.52}$$

With $b < 20 - 24$ we get perturbative Yukawa couplings ($\alpha_{y_\nu} = |y_\nu|^2 / 4\pi < 1$).
In the $n = 3$ case, the general parametrisation for an orthogonal complex matrix is

$$\mathcal{O} = \pm \begin{pmatrix} 1 & 0 & 0 \\ 0 & c_{\omega_x} & s_{\omega_x} \\ 0 & -s_{\omega_x} & c_{\omega_x} \end{pmatrix} \begin{pmatrix} c_{\omega_y} & 0 & s_{\omega_y} \\ 0 & 1 & 0 \\ -s_{\omega_y} & 0 & c_{\omega_y} \end{pmatrix} \begin{pmatrix} c_{\omega_z} & s_{\omega_z} & 0 \\ -s_{\omega_z} & c_{\omega_z} & 0 \\ 0 & 0 & 1 \end{pmatrix}. \tag{3.53}$$

The first column of the Yukawa matrix can be set to zero if $s_{\omega_y} + c_{\omega_y} s_{\omega_z} = 0$, which is trivially achieved if ω_y, $\omega_z = 0$. In this case,

$$y_{\alpha 1} = 0, \quad y_{\alpha 2} = c_{\omega_x} + s_{\omega_x}, \quad y_{\alpha 3} = -s_{\omega_x} + c_{\omega_x}. \tag{3.54}$$

The sterile HNF mass m_{ψ_1} does not enter the computation. Taking $m_{\psi_2} \simeq m_{\psi_3}$ in the desired range, we obtain

$$|y_{\alpha 2}| \simeq |y_{\alpha 3}| \sim \frac{\mathrm{e}^{b_x}}{2} \left(10^{-10} - 10^{-8}\right) \tag{3.55}$$

and again we get perturbative Yukawa couplings (possibly with a phase between $y_{\alpha 2}$ and $y_{\alpha 3}$) choosing $b_x < 20 - 24$.
The $n = 4$ case is analogous to $n = 3$, since $\mathcal{O}$ is 4×3 and can be expressed just like the result of (3.53) with a row of zeroes on top. This just adds a zero column to y_ν, yielding

$$y_{\alpha 1} = y_{\alpha 2} = 0, \quad |y_{\alpha 3}| \simeq |y_{\alpha 4}| \sim \frac{\mathrm{e}^{b_x}}{2} \left(10^{-10} - 10^{-8}\right). \tag{3.56}$$

3.3 Thermal target for iDM

There is fairly wide literature (e.g. [49] and references therein) devoted to the calculation of a thermal target, by which we mean a region in parameter space in which the observed DM abundance is obtained from the model at hand. This target requires a minimum interaction rate between DM and the SM, for which the pure inelastic dark matter model is particularly well suited. Indeed, as we hinted at the end of section 3.1.1, we can hypothesise that inelastic collisions with SM particles, which constitute the mechanism solving direct detection discrepancies, be also responsible for the leading annihilation process (*coannihilation*) in the early universe, via the s-channel diagram[2]

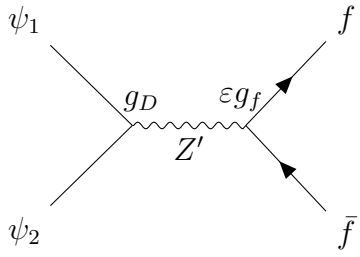

Being the heavier species ψ_2 subject to Boltzmann suppression during freeze-out, the annihilation rate for this process must be high enough to compensate, and this is possible to achieve with the freedom we have in choosing g_D.
The instability of the heavier state also shuts off completely indirect detection at late time, evading experimental bounds from that searching area. In particular, the bound from CMB on s-wave annihilation, which excludes thermal DM lighter than ~ 10 GeV, is lifted and we can consider the velocity-independent coannihilation cross section [50]

$$\sigma v(\psi_1 \psi_2 \to e^+ e^+) \simeq \frac{4\pi\epsilon^2 \alpha_{\mathrm{em}} \alpha_D \left(m_{\psi_1} + m_{\psi_2}\right)^2}{\left[\left(m_{\psi_1} + m_{\psi_2}\right)^2 - m_{Z'}^2\right]^2 + m_{Z'}^2 \Gamma_{Z'}^2}, \tag{3.57}$$

[2]We are excluding *secluded annihilation*, i.e. the process $\psi_i \psi_i \to Z' Z'$ through t-channel exchange of ψ_j, by taking the dark photon heavier than both ψ_1 and ψ_2.

where $\Gamma^2_{Z'}$ is the width of the dark photon. A resonant behaviour is obtained for $m_{Z'} = m_{\psi_1} + m_{\psi_2}$, so most studies consider Z' heavy enough to avoid it.
The method by which one obtains the thermal target was basically outlined in section 1.3. A system of coupled Boltzmann equations (1.18) for ψ_1 and ψ_2 must be solved, taking into account also the ψ_2 depletion due to it decaying to ψ_1. While we refer the reader to [50] for all the details, we find it appropriate to display here the form of the Boltzmann system:

$$\frac{\mathrm{d}Y_{\psi_1,\psi_2}}{\mathrm{d}x} = -\frac{\lambda_\mathrm{A}}{x^2}\left(Y_{\psi_1}Y_{\psi_2} - Y^\mathrm{eq}_{\psi_1}Y^\mathrm{eq}_{\psi_2}\right) \pm x\lambda_\mathrm{D}\left(Y_{\psi_2} - \frac{Y^\mathrm{eq}_{\psi_2}}{Y^\mathrm{eq}_{\psi_1}}Y_{\psi_1}\right) \pm \frac{\lambda_\mathrm{S}}{x^2}Y^\mathrm{eq}_f\left(Y_{\psi_2} - \frac{Y^\mathrm{eq}_{\psi_2}}{Y^\mathrm{eq}_{\psi_1}}Y_{\psi_1}\right), \quad (3.58)$$

with

$$\lambda_\mathrm{A} = \frac{s(m_{\psi_2})}{H(m_{\psi_2})}\langle\sigma v(\psi_1\psi_2 \to f\bar{f})\rangle, \quad (3.59)$$

$$\lambda_\mathrm{S} = \frac{s(m_{\psi_2})}{H(m_{\psi_2})}\langle\sigma v(\psi_2 f \to \psi_1 f)\rangle, \quad (3.60)$$

$$\lambda_\mathrm{D} = \frac{\langle\Gamma(\psi_2 \to \psi_1 f\bar{f})\rangle}{H(m_{\psi_2})}. \quad (3.61)$$

The value we are interested in is $Y^\infty_{\psi_1}$ at freeze-out instant $x_\mathrm{F} \simeq 20$, which enters the expression of the relic abundance

$$\Omega_{\psi_1} = \frac{m_{\psi_1}s_0Y^\infty_{\psi_1}}{\rho_\mathrm{cr}}. \quad (3.62)$$

The obtained value is then equated to the observed $\Omega_\mathrm{DM}h^2 = 0.12$ (from [4]). This gives a hypersurface in the parameter space, which can be parametrised as $y = y(m_{\psi_1})$, where

$$y \equiv \varepsilon^2\alpha_D\left(\frac{m_{\psi_1}}{m_{Z'}}\right)^4 \quad (3.63)$$

as suggested by the parameter dependence in (3.57) for relatively small mass differences Δ_{21}. The high dimensionality of the parameter space can be taken care of by slicing it for specific values of α_D and Δ_{21} and considering the $y = y(m_{\psi_1})$ curves for various choices of $n \equiv m_{Z'}/m_{\psi_1}$. This was done in [49], of which we present the results in figure 3.1.

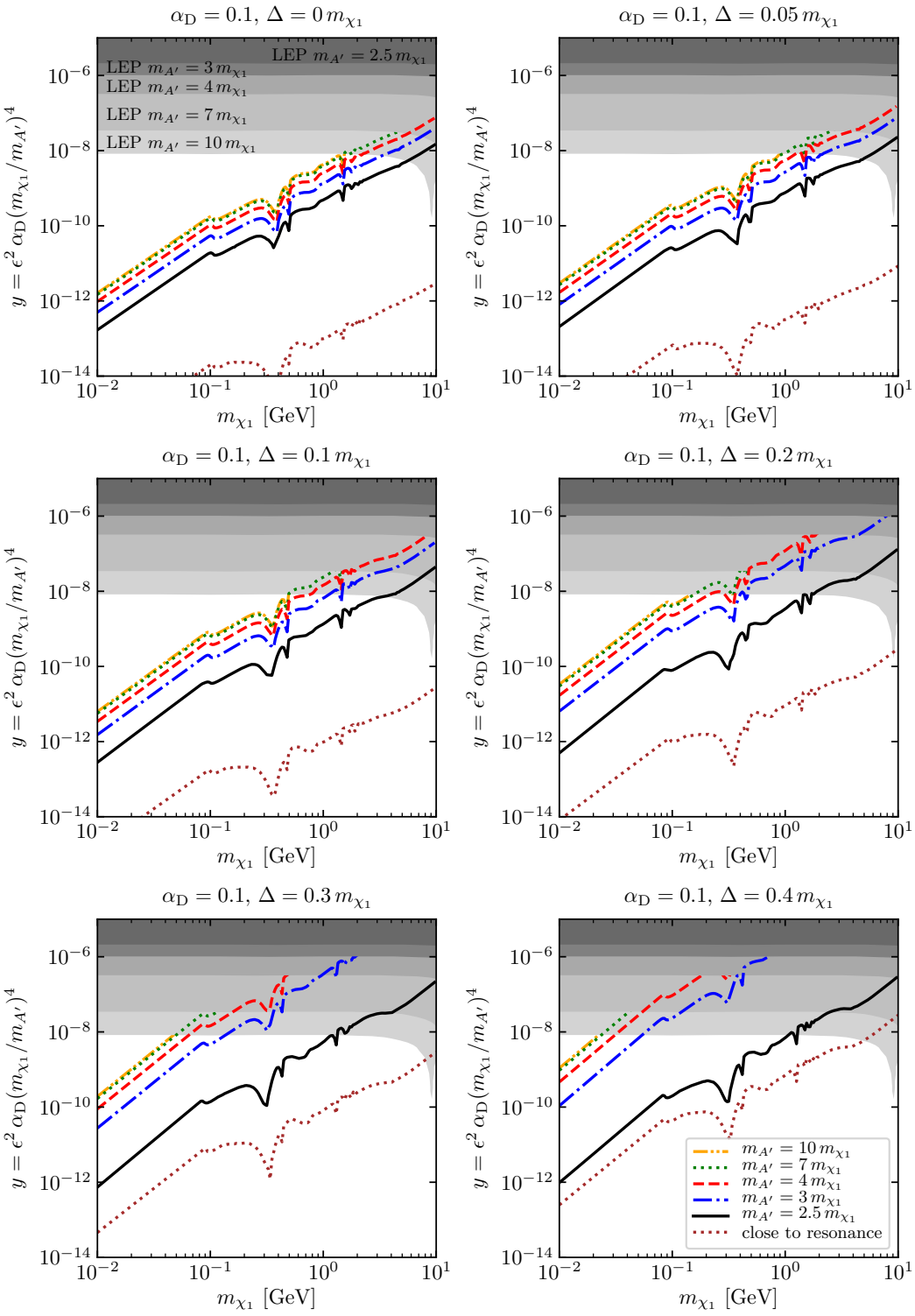

Figure 3.1: Calculated thermal targets for the iDM model, at various mass differences $\Delta \equiv \Delta_{21} m_{\psi_1}$ and mediator mass ratios $m_{Z'}/m_{\chi_1} \equiv n$ (the usual notation for DM candidates χ_i is employed instead of ψ_i). Model-independent LEP bounds on the kinetic mixing ε are shaded in grey. Figure taken from [49].

Chapter 4

Dark photon phenomenology at ICARUS

The final part of this thesis work consists in a preliminary analysis for an experimental test of the previously analysed rich dark sector models. The context is a terrestrial search for dark sector interactions at Fermilab, using the data from the Short-Baseline Neutrino program. In particular, we will consider the production and semi-visible decay chain of dark photons, and calculate the expected event rate in the ICARUS-T600 detector. Section 4.1 deals with the predictions related to the physics of the model alone. In section 4.2 a brief review of the experiment history and design is given, while section 4.3 contains the rough prediction of the total event rate for the considered process.

4.1 Processes involving the dark photon

This section deals with the task of extracting phenomenological consequences from the models presented in section 3.1. In particular, we will show how dark photons may be produced in extracted beams, and calculate its semi-visible decay rates. For the latter, we will use textbook techniques of QFT at tree level. Kinematic formulae relevant for the two-body and three-body decays are taken from [35]. The calculations will be carried out first in the two-HNF model from section 3.1.1. This way, we can highlight the effects of the Majorana nature of ψ_1 and ψ_2, of the relative Majorana phase φ, and of the dark charges, all of which are turned off to some degree in the other models. How the results get modified to obtain the different benchmark points will be discussed at the end. The calculations should be general enough to be easily adapted to competing models involving dark vector bosons and Majorana neutrinos.

4.1.1 Z' production

In beam-dump experiments, a high-intensity proton beam is made to hit an extended fixed target. The resulting secondary particles, in particular mesons, pass through an empty volume, where they propagate until they decay into lighter states. While this setup is usually employed to generate a neutrino beam through the decay of charged meson (e.g. $\pi^+ \to \mu^+\nu_\mu$), a fair amount of photons from decays of neutral mesons is produced (e.g. $\pi^0 \to \gamma\gamma$). If kinetic mixing comes into play and the meson mass is high enough, the meson can actually decay to $\gamma Z'$, with a branching ratio depending on the magnitude of the kinetic mixing ε. Now, while the meson production is mediated by the strong

interaction and a sizeable amount of mesons is guaranteed per collision, the meson decays into photons are mostly loop-level electromagnetic, with low branching ratios (excluding the neutral pion for which the 2γ branch is dominant). The production of Z' is therefore suppressed both by ε and because of the alternative decay channels. However, the rarity of such decays is compensated by the sheer amount of meson-producing collisions at the target.
An argument for considering kaons, in the weak eigenstate K_L^0, is the following: they are the longest-lived neutral meson produced in beam-dump facilities, with mean life [51]

$$\tau_{K_L^0} = (5.116 \pm 0.021) \times 10^{-8}\ \text{s}, \tag{4.1}$$

meaning they decay fairly away from the target, with low backgrounds from other sources. The corresponding mass eigenstate has $m_{K^0} \simeq 498$ MeV, meaning that, while being light enough to be produced from high-intensity beams, they are still able to decay to on-shell $O(100)$ MeV dark photons.
The branching ratio for the $\gamma Z'$ channel is computed to be [52]

$$\text{BR}_{K_L^0 \to \gamma Z'} \simeq 10^{-3}\varepsilon^2 \left(1 - \frac{m_{Z'}^2}{m_{K^0}^2}\right)^3. \tag{4.2}$$

4.1.2 $Z' \to \psi_i \psi_j$

Under the assumption that $m_{Z'} > m_{\psi_i}$ for all i, we proceed with the tree-level calculation for the unpolarised decay rate of Z' into a pair of heavy Majorana neutrinos, through a dark current like the one in (3.8), whose general expression is

$$J_D^\mu = V_{ij}\overline{\psi_i}\gamma^\mu\psi_j + A_{ij}\overline{\psi_i}\gamma^\mu\gamma^5\psi_j. \tag{4.3}$$

Majorana fermions have only one set of creation and annihilation operators $\{a_k^\dagger, a_k\}$ unlike Dirac fermions, which have two: $\{b_k^\dagger, b_k\}$ for particles and $\{c_k^\dagger, c_k\}$ for antiparticles. This leads to different contractions with external states. If ψ_i and ψ_j were Dirac fermions, the normal-mode decomposition, written schematically as

$$\psi \sim \sum_k \left(b_k u_k + c_k^\dagger v_k\right) \tag{4.4}$$

would give, for the process $Z' \to \psi_i\overline{\psi_j}$,

$$\left\langle \psi_i\overline{\psi_j}\right| \left(\overline{\psi_i}\Gamma\psi_j + \overline{\psi_j}\Gamma\psi_i\right) |0\rangle = \langle 0|\, \overline{u_i}\Gamma v_j\, |0\rangle\,, \tag{4.5}$$

and $\langle 0|\, \overline{u_j}\Gamma v_i\, |0\rangle$ for the conjugate process $Z' \to \psi_j\overline{\psi_i}$.[1] Here instead we will consider ψ_i and ψ_j to be Majorana fields, decomposed as

$$\psi \sim \sum_k \left(a_k u_k + a_k^\dagger v_k\right), \tag{4.6}$$

and therefore the contraction with external states for the process $Z' \to \psi_i\psi_j$ gives

$$\langle \psi_i\psi_j| \left(\overline{\psi_i}\Gamma\psi_j + \overline{\psi_j}\Gamma\psi_i\right) |0\rangle = \langle 0|\, \left(\overline{u_i}\Gamma v_j + \overline{u_j}\Gamma v_i\right) |0\rangle\,. \tag{4.7}$$

[1] The symbol Γ is used as a shorthand for the relevant product of gamma matrices with its coefficient.

The case with one Dirac fermion and one Majorana fermion is analogous to the one with two Dirac fermions.
Translating this to the language of Feynman rules, the S-matrix element for the tree-level process

$$Z'(p) \to \psi_i(k_i) + \psi_j(k_j)$$

where ψ_i and ψ_j are Majorana fermions, is given by the sum of the following two diagrams:

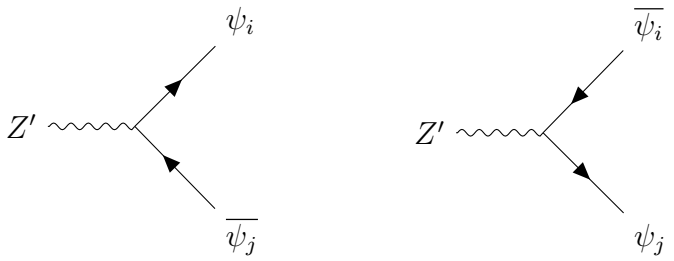

$$i\mathcal{M} = \overline{u}(k_i) i g_D \epsilon_\mu(p) \gamma^\mu \big(V_{ij} + A_{ij}\gamma^5\big) v(k_j) + (i \leftrightarrow j). \tag{4.8}$$

We then take the modulus squared, sum over the final spins and average over the initial polarisation states. In doing this, the mixed terms from the two diagrams cancel against each other, although this is not trivial: one has to work out the spin sums using the additional formulae valid only for Majorana fermions (as found e.g. in [53]).
This leads to

$$\begin{aligned}\overline{|\mathcal{M}|^2} = \frac{1}{3} g_D^2 \left(-g^{\mu\nu} + \frac{p^\mu p^\nu}{m_{Z'}^2}\right) \mathrm{tr}\left[\left(\not{k}_j - m_j\right) \gamma_\mu \left(V_{ij}^* + A_{ij}^* \gamma^5\right)\right. \\ \left. \times \left(\not{k}_i + m_i\right) \gamma_\nu \left(V_{ij} + A_{ij}\gamma^5\right)\right] + (i \leftrightarrow j).\end{aligned} \tag{4.9}$$

Using standard trace identities, and getting rid of p using momentum conservation ($p = k_i + k_j$), we come to the expression

$$\begin{aligned}\overline{|\mathcal{M}|^2} = \frac{8}{3} g_D^2 \left\{ \left(|V_{ij}|^2 + |A_{ij}|^2\right) \left[2 k_i \cdot k_j + \frac{\left(m_i^2 + m_j^2\right) k_i \cdot k_j + 2 m_i^2 m_j^2}{m_{Z'}^2}\right]\right. \\ \left. + \left(|V_{ij}|^2 - |A_{ij}|^2\right) \left[4 m_i m_j - \frac{\left(m_i^2 + m_j^2 + 2 k_i \cdot k_j\right) m_i m_j}{m_{Z'}^2}\right]\right\}.\end{aligned} \tag{4.10}$$

Fermi's golden rule for the 2-body decay reads

$$\mathrm{d}\Gamma = \frac{1}{32\pi^2} \overline{|\mathcal{M}|^2} \frac{|\mathbf{k}_i|}{m_{Z'}^2} \mathrm{d}\Omega. \tag{4.11}$$

Being the Z' unpolarised, we have no dependence on the angles in its rest frame. Two-body kinematics gives

$$|\mathbf{k}_i| = |\mathbf{k}_j| = \frac{\left[\left(m_{Z'}^2 - (m_1 + m_2)^2\right)\left(m_{Z'}^2 - (m_1 - m_2)^2\right)\right]}{2 m_{Z'}}. \tag{4.12}$$

Expressing the dot product as

$$k_i \cdot k_j = \frac{(k_i + k_j)^2 - k_i^2 - k_j^2}{2} = \frac{m_{Z'}^2 - m_i^2 - m_j^2}{2}, \tag{4.13}$$

we arrive, after some algebra, at the general result

$$\Gamma_{Z'\to\psi_i\psi_j} = \frac{g_D^2}{6\pi} m_{Z'} \sqrt{\left[1-\left(\frac{m_i-m_j}{m_{Z'}}\right)^2\right]\left[1-\left(\frac{m_i+m_j}{m_{Z'}}\right)^2\right]} \times \left\{ \left(|V_{ij}|^2+|A_{ij}|^2\right)\left[1-\frac{1}{2}\frac{m_i^2+m_j^2}{m_{Z'}^2}-\frac{1}{2}\left(\frac{m_i^2-m_j^2}{m_{Z'}^2}\right)^2\right] + 3\left(|V_{ij}|^2-|A_{ij}|^2\right)\frac{m_i m_j}{m_{Z'}^2}\right\}. \quad (4.14)$$

For $i \neq j$, the coefficients in (3.8) give

$$\Gamma_{Z'\to\psi_2\psi_1} = \frac{\left(g_D Q_V s_{2\theta}\right)^2}{6\pi} m_{Z'} \times \sqrt{\left[1-\left(\frac{m_{\psi_2}-m_{\psi_1}}{m_{Z'}}\right)^2\right]\left[1-\left(\frac{m_{\psi_2}+m_{\psi_1}}{m_{Z'}}\right)^2\right]} \times \left[1-\frac{1}{2}\frac{m_{\psi_2}^2+m_{\psi_1}^2}{m_{Z'}^2}-\frac{1}{2}\left(\frac{m_{\psi_2}^2-m_{\psi_1}^2}{m_{Z'}^2}\right)^2-3c_{2\varphi}\frac{m_{\psi_2}m_{\psi_1}}{m_{Z'}}\right], \quad (4.15)$$

whereas, for $i = j$,

$$\Gamma_{Z'\to\psi_i\psi_i} = \frac{g_D^2\left(Q_A \pm Q_V c_{2\theta}\right)^2}{24\pi} m_{Z'}\left(1-4\frac{m_{\psi_i}^2}{m_{Z'}^2}\right)^{3/2}, \quad (4.16)$$

where the upper sign refers to ψ_2 and the lower sign to ψ_1.

Benchmarks

In the iDM model from section 3.1.1, we set $\theta = \pi/4$, $\phi = \pi/2$, $Q_A = 0$, which kills off the diagonal terms, and thus the decay (4.16). The axial coupling is also turned off. Setting $Q_V = 1$, (4.15) becomes, in terms of the relevant parameters ($r_i \equiv m_{\psi_i}/m_{Z'}$),

$$\Gamma^{(\text{iDM})}_{Z'\to\psi_2\psi_1} = \frac{2}{3}\alpha_D m_{Z'}\left[1+2r_1-\frac{3}{2}\Delta_{21}\left(\Delta_{21}+2\right)r_1^2+O(r_1^3)\right]. \quad (4.17)$$

We now turn to the 3HNF models, from section 3.1.2. The mixed-iDM model, using (3.24) for J_D^μ, contains the Dirac fermion Ψ_2, which means that the decay rate gets halved with respect to the full Majorana case. This time we also have the $i = j$ case, for which we modify (4.16) accordingly:

$$\Gamma^{(\text{mixed}-\text{iDM})}_{Z'\to\Psi_2\psi_1} = \frac{1}{2}s_\alpha \Gamma^{(\text{iDM})}_{Z'\to\psi_2\psi_1}, \quad (4.18)$$

$$\Gamma^{(\text{mixed}-\text{iDM})}_{Z'\to\Psi_2\Psi_2} = \frac{1}{3}c_\alpha\alpha_D m_{Z'}\left(1-4r_2^2\right)^{3/2}. \quad (4.19)$$

The result for the three Majorana fermion models (BP4, BP5), as well as that for the i2DM model (BP3) can be deduced in a similar fashion from the general case.

4.1.3 Z'-mediated $\psi_2 \to \psi_1 \ell^- \ell^+$

We set out to calculate the three-body decay of the heavier Majorana state ψ_2 into the lighter one ψ_1 and a SM lepton-antilepton pair, at tree level. Following the reasoning of the previous section for what concerns the Majorana nature of fermions, and assuming a small momentum transfer from ψ_2 to the lepton pair ($q \ll m_{Z'}$), we see that the matrix element for the process

$$\psi_2(p) \to \psi_1(k_1) + \ell^-(k_2) + \ell^+(k_3)$$

is given by the sum of the diagrams:

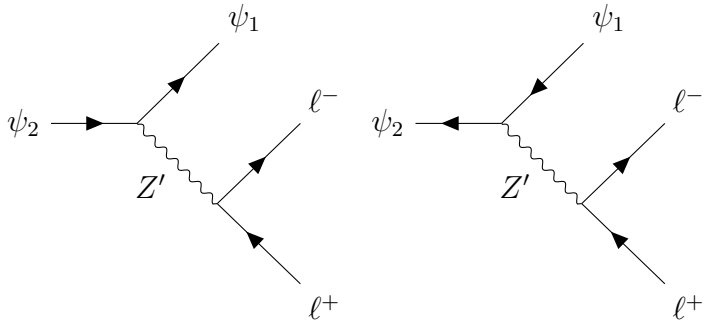

$$\begin{aligned} i\mathcal{M} = {} & \overline{u}(k_1)\, ig_D\gamma^\mu \left(V_{12} + A_{12}\gamma^5\right)\, u(p) \left(\frac{-i}{m_{Z'}^2}\right) \overline{u}(k_2)\, i\varepsilon e\gamma_\mu\, v(k_3) \\ & + \overline{v}(p)\, ig_D\gamma^\mu \left(V_{12} + A_{12}\gamma^5\right)\, v(k_1) \left(\frac{-i}{m_{Z'}^2}\right) \overline{u}(k_2)\, i\varepsilon e\gamma_\mu\, v(k_3). \quad (4.20) \end{aligned}$$

Taking the modulus squared and summing over the final spins and averaging over the initial ones, we get

$$\begin{aligned} \overline{|\mathcal{M}|^2} = {} & \frac{1}{2}\frac{\left(g_D\varepsilon e\right)^2}{m_{Z'}^4} \operatorname{tr}\left[\left(\not{k}_3 - m_\ell\right)\gamma_\mu\left(\not{k}_2 + m_\ell\right)\gamma_\nu\right] \\ & \times \Big\{\operatorname{tr}\left[\left(\not{p} + m_2\right)\gamma^\mu\left(V_{12}^* + A_{12}^*\gamma^5\right)\left(\not{k}_1 + m_1\right)\gamma^\nu\left(V_{12} + A_{12}\gamma^5\right)\right] \\ & + \operatorname{tr}\left[\left(\not{k}_1 - m_1\right)\gamma^\mu\left(V_{12}^* + A_{12}^*\gamma^5\right)\left(\not{p} - m_2\right)\gamma^\nu\left(V_{12} + A_{12}\gamma^5\right)\right]\Big\}. \quad (4.21) \end{aligned}$$

Just like in the previous calculation, the mixed terms get cancelled. Using standard trace identities we are led to

$$\begin{aligned} \overline{|\mathcal{M}|^2} = {} & \frac{32\left(g_D\varepsilon e\right)^2}{m_{Z'}^4} \\ & \times \Big\{\left(|V_{12}|^2 + |A_{12}|^2\right)\left[(p\cdot k_3)(k_1\cdot k_2) + (p\cdot k_2)(k_1\cdot k_3) + m_\ell^2(p\cdot k_1)\right] \\ & + \left(|V_{12}|^2 - |A_{12}|^2\right)\left[-m_{\psi_1}m_{\psi_2}(k_2\cdot k_3 + 2m_\ell^2)\right]\Big\}. \quad (4.22) \end{aligned}$$

To simplify, we set $m_\ell = 0$. Substituting the coefficients in (3.8) for V_{12} and A_{12} we get

$$\overline{|\mathcal{M}|^2} = \frac{32\left(g_D\varepsilon e Q_V \sin 2\theta\right)^2}{m_{Z'}^4} f(p, k_1, k_2, k_3), \quad (4.23)$$

where

$$f(p, k_1, k_2, k_3) = (p\cdot k_3)(k_1\cdot k_2) + (p\cdot k_2)(k_1\cdot k_3) + \cos 2\varphi\, m_{\psi_1}m_{\psi_2}(k_2\cdot k_3). \quad (4.24)$$

The dot products can be expressed in terms of the Dalitz variables

$$m_{ij}^2 \equiv (k_i + k_j)^2, \qquad i, j = 1, 2, 3 \tag{4.25}$$

and of the Majorana fermion masses m_{ψ_1}, m_{ψ_2}, to obtain

$$f(m_{12}, m_{23}, m_{13}) = \frac{1}{4}\left[\left(m_{12}^2 - m_{\psi_1}^2\right)\left(m_{\psi_2}^2 - m_{12}^2\right) + \left(m_{13}^2 - m_{\psi_1}^2\right)\left(m_{\psi_2}^2 - m_{13}^2\right) + 2\cos 2\varphi\, m_{\psi_1} m_{\psi_2} m_{23}^2\right]. \tag{4.26}$$

Next, we use momentum conservation, in the form

$$m_{12}^2 + m_{23}^2 + m_{13}^2 = m_{\psi_1}^2 + m_{\psi_2}^2, \tag{4.27}$$

to get rid of m_{13} in (4.26):

$$f(m_{12}, m_{23}) = \frac{1}{4}\left[-2m_{12}^4 - m_{23}^4 - 2m_{12}^2 m_{23}^2 + 2\left(m_{\psi_1}^2 + m_{\psi_2}^2\right) m_{12}^2 + \left(m_{\psi_1}^2 + m_{\psi_2}^2 + 2\cos 2\varphi\, m_{\psi_1} m_{\psi_2}\right) m_{23}^2 + 2m_{\psi_1}^2 m_{\psi_2}^2\right]. \tag{4.28}$$

We are now ready to use Fermi's golden rule for the differential width in terms of the Dalitz variables:

$$\mathrm{d}\Gamma = \frac{1}{(2\pi)^3}\frac{1}{32 m_{\psi_2}^3}\overline{|\mathcal{M}|^2}\,\mathrm{d}m_{12}^2\,\mathrm{d}m_{23}^2. \tag{4.29}$$

To simplify the notation, we set

$$r \equiv \frac{m_{\psi_1}}{m_{\psi_2}}, \qquad x \equiv \frac{m_{12}^2}{m_{\psi_2}^2}, \qquad y \equiv \frac{m_{23}^2}{m_{\psi_2}^2}. \tag{4.30}$$

Now (4.29) reads

$$\mathrm{d}\Gamma = \frac{\left(g_D \varepsilon e Q_V \sin 2\theta\right)^2}{32\pi^3 m_{Z'}^4} m_{\psi_2}^5 \left[-2x^2 - y^2 - 2xy + 2(1 + r^2)x + (1 + r^2 + 2\cos 2\varphi\, r)y + 2r^2\right] \mathrm{d}x\,\mathrm{d}y. \tag{4.31}$$

The last step involves integration over the Dalitz plot. The bounds of integration are

$$x_{\min} = r^2, \qquad x_{\max} = 1, \tag{4.32}$$

$$y_{\min} = 0, \qquad y_{\max} = 1 - x - \frac{r^2}{x} + r^2. \tag{4.33}$$

The final result is given in terms of the mass ratio r:

$$\Gamma_{\psi_2 \to \psi_1 \ell^- \ell^+} = \frac{\left(g_D \varepsilon e Q_V \sin 2\theta\right)^2}{192\pi^3 m_{Z'}^4} m_{\psi_2}^5 \left[1 + 4r^2 + 24r^4 \ln r + 2\cos 2\varphi\left(r + 9r^3 + 12r^3 \ln r\right) + O(r^5)\right]. \tag{4.34}$$

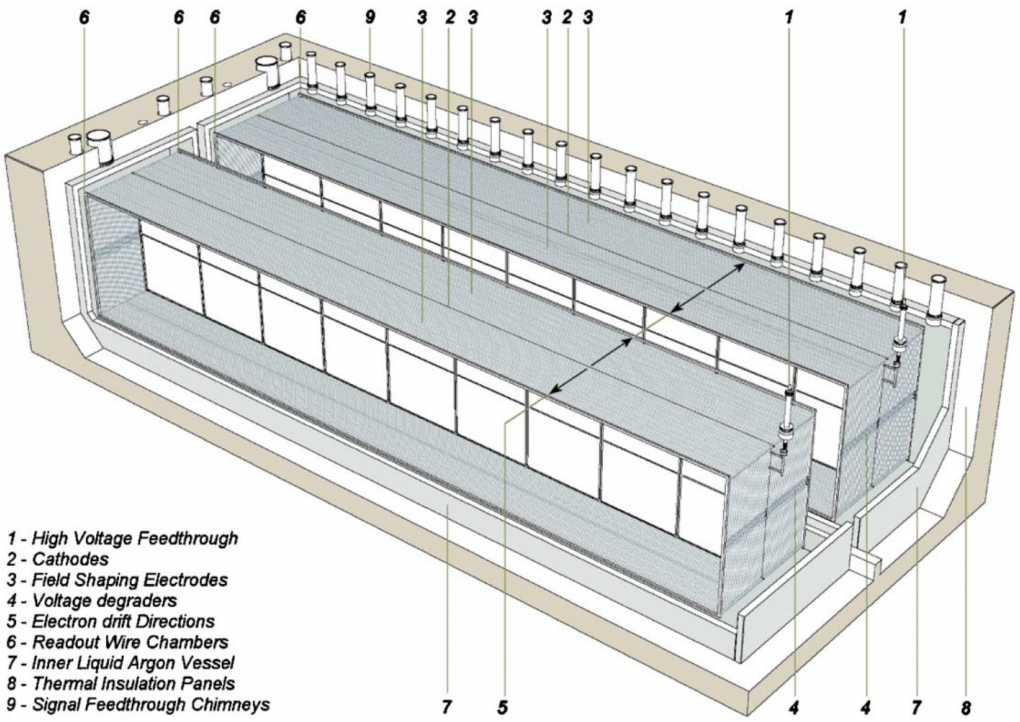

Figure 4.1: Artist cutaway view of the ICARUS-T600 detector. Figure taken from [54].

Benchmarks

To specialise the result in (4.34) to the various models from section 3.1, we set $\theta = \pi/4$, $\varphi = \pi/2$, $Q_A = 0$, $Q_V = 1$, and use the relevant formulae for the dark current. For the models involving Dirac or pseudo-Dirac fermions, either in the final or initial state, the decay rates get halved. For the iDM and mixed-iDM cases, we obtain ($r_i \equiv m_{\psi_i}/m_{Z'}$):

$$\Gamma^{\text{iDM}}_{\psi_2 \to \psi_1 \ell^- \ell^+} = \frac{\alpha_D \alpha_{\text{em}} \varepsilon^2}{12\pi} r_1^4 m_{\psi_1} (1+\Delta_{21})^5 \left[1 + 4\,(1+\Delta_{21})^{-2} + o\left((1+\Delta_{21})^{-4}\right)\right], \quad (4.35)$$

$$\Gamma^{\text{mixed-iDM}}_{\Psi_2 \to \psi_1 \ell^- \ell^+} = \frac{1}{2} s_\alpha \Gamma^{\text{iDM}}_{\psi_2 \to \psi_1 \ell^- \ell^+}. \quad (4.36)$$

Similar results hold for the other benchmark points.

4.2 ICARUS at the Fermilab Short-Baseline Neutrino program

ICARUS (Imaging Cosmic And Rare Underground Signals) [54] [55] is the first large-scale experiment based on LAr-TPC (Liquid Argon Time Projection Chamber) technology. As such, it can observe neutrino interactions at energies from few keV to hundreds of GeV, providing 3D imaging and calorimetric reconstruction of incoming ionising particles.
The ICARUS-T600 detector is composed of two modules, essentially huge tanks ($3.6 \times 3.9 \times 19.6$ m^3 each) filled with liquid argon (760 tons total, of which 476 available for interactions), whose inside is instrumented with charged wires arranged along three planes, generating a uniform 500 V/cm electric field. When a weakly interacting neutral particle strikes an Ar atom, charged particles are released, which in turn ionises nearby atoms, creating a streak of electrons that drifts towards the nearest wire, generating signal. The

Figure 4.2: View of the ICARUS detector inner TPC during its overhaul, with the cathode plane on the left and the wire planes, along with the PMTs, on the right. Photo: CERN.

drifting time is also measured, using PMT-captured scintillation from the interactions as a trigger. The result is a complete 3D reconstruction of the event.
Proposed originally by C. Rubbia back in 1977, the experiment was first run at LNGS from 2010 to 2013, where it observed neutrino oscillations, particularly as part of the CNGS project alongside OPERA. It then underwent a period of overhaul at CERN, and was then transported overseas to Fermilab, where it is now part of the Short Baseline Neutrino program along with SBND and MicroBooNE, and has been taking measurements since 2021. ICARUS T-600 is exposed to both the Booster neutrino beam (BNB) and the neutrino at the Main Injector (NuMI) beam. The main goal at Fermilab is to study the sterile neutrino hypothesis and clarify the low-energy anomalies from LSND and MiniBooNE.
We now give some quantitative details for the analysis in the next section. The BNB consists of an 8 GeV proton beam impinging on a beryllium target, with all the SBN detectors, among which ICARUS is the farthest away (600 m from target), located along the beam axis. On the other hand, the NuMI beam is produced by striking 120 GeV protons on a graphite target, and the detectors are all off-axis, with ICARUS being 803 m away from the target at an angle of 0.097 rad (5.5°). The active volume for each chamber is $2.67 \times 2.86 \times 17.00$ m^3.

4.3 Calculation of the expected number of events

To estimate the number of heavy neutral particles from the semi-visible dark photon model that can produce a signal inside ICARUS, we first considered the meson production from the BNB and the NuMI beam. By the arguments outlined in section 4.1.1, we restricted our analysis to the K_L^0, and considered the decay chain $K_L^0 \to \gamma Z'$, then $Z' \to \psi_2\psi_1$, with ψ_2 entering the detector and decaying to $\psi_1 e^+e^-$, with the electron-

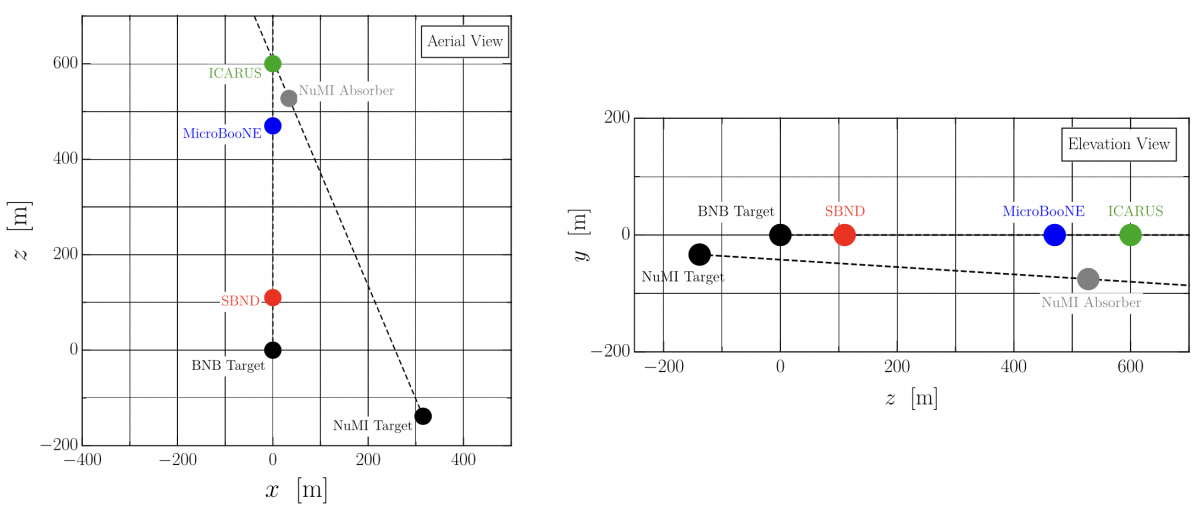

Figure 4.3: Map of the Fermilab SBN experiments, aerial (left) and elevation (right) view, centered at the BNB target. Figure taken from [56].

positron pair capable of leaving tracks. The multiple decay stages, together with the geometry of the experiment, required a careful simulation of the decay events and propagation to get any meaningful result. The procedure we used is inspired by [56], which uses kaons at Fermilab to test a model involving a dark scalar.

Algorithm description

The master formula for the event rate is the following:

$$R = \epsilon_{\text{det}} N_{\text{pot}} \frac{\rho N_A L}{A} \sigma_{pA} \mathcal{P}. \tag{4.37}$$

It can be broken down into three parts.

- The terms which depend on the experimental setup include the detector efficiency ϵ_{det}, the number of protons on target (per year) N_{pot}, the density of the target ρ and its length L, while A is the target mass number. For our simulations, we used $\epsilon_{\text{det}} \simeq 10\%$, $N_{\text{pot}} \simeq 5.7 \times 10^{20}$/year, $\rho_{\text{NuMI}} = 1.78$ g/cm^3 (POCO graphite) and $\rho_{\text{BNB}} = 1.85$ g/cm^3 (beryllium).

- The total cross sections σ_{pA} for the proton-nucleus collision were calculated through a `Pythia` [57] Monte Carlo simulation, with 10^6 events. By default, for collisions involving nuclei, the `Pythia` engine employs the Angantyr model [58]. The result was $(3.640 \pm 0.003) \times 10^2$ mb for the NuMI beam and $(2.716 \pm 0.002) \times 10^2$ mb for the BNB.

- The symbol $\mathcal{P}$ denotes the probability that the produced K_L^0 actually generates a ψ_2 decay inside ICARUS. To estimate it, a combination of `Python` and `Mathematica` scripts were used to manipulate the `Pythia` output, consisting in the 4-momenta of the outgoing kaons.

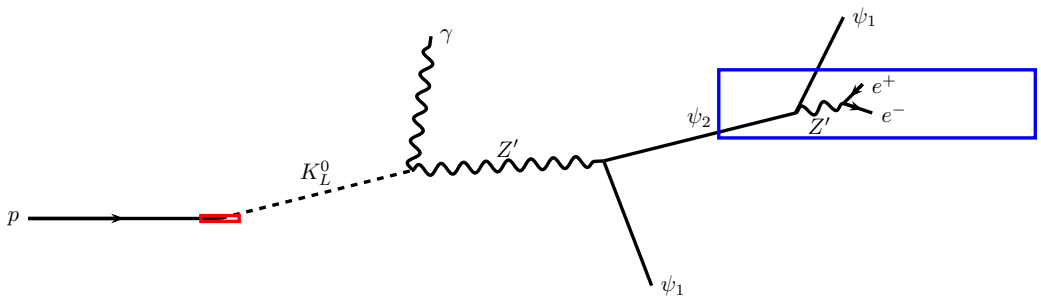

Figure 4.4: Schematic drawing of the semi-visible dark photon production and decay at Fermilab (not to scale). The red rectangle denotes the beam target, while the blue rectangle represents the active volume of ICARUS.

Let us go into some more detail about the calculation of $\mathcal{P}$, which can be expressed as the product

$$\mathcal{P} = Y_{K_L^0} \mathrm{BR}_{K_L^0 \to \gamma Z'} f_{\mathrm{det}} f_{\mathrm{in}}. \tag{4.38}$$

Here, $Y_{K_L^0}$ is the average kaon yield per collision, estimated by `Pythia` to be around 0.92 for the NuMI beam and 0.34 for the BNB. The branching ratio is given by (4.2). Clearly, we are assuming that no other decay channels are available for Z' and ψ_2 besides those calculated in sections 4.1.2 and 4.1.3. The last two factors require a separate treatment. The factor f_{det} is the fraction of kaons, assumed to have branched to $\gamma Z'$, and therefore bound to go down the full decay chain, resulting in a ψ_2 hitting the active detector volume. To get this number, we first have to calculate, for each kaon, the position $\mathbf{r}_2$ at which the ψ_2 is generated and its velocity $\boldsymbol{\beta}_2 \equiv \boldsymbol{\beta}_{\psi_2}|_{\mathrm{lab}}$ (in units of c) in the laboratory frame. The position can be expressed as

$$\mathbf{r}_2 = \mathbf{r}_0 + \hat{\boldsymbol{\beta}}_K|_{\mathrm{lab}} \ell_1 + \hat{\boldsymbol{\beta}}_{Z'}|_{\mathrm{lab}} \ell_2, \tag{4.39}$$

where the hatted quantities denote unit vectors, while ℓ_1 and ℓ_2 respectively denote the travel distances of the K_L^0 and Z'. With the exception of $\mathbf{r}_0$, which points at the beam target and is taken as the origin of the coordinate system (with the laboratory z axis in the direction of the beam), all other quantities in (4.39) are statistically simulated. In particular, the velocity vectors $\boldsymbol{\beta}_i$ are first generated in a random direction[2] $\hat{\mathbf{n}}_i^*$ (a star denotes that the quantity is taken in the rest frame of the parent particle), then boosted to the lab frame, according to the following equations:

$$\boldsymbol{\beta}^*_{Z'} = \frac{\mathbf{p}^*_{Z'}}{E^*_{Z'}} = \frac{m_K^2 - m_{Z'}^2}{m_K^2 + m_{Z'}^2} \hat{\mathbf{n}}_1, \tag{4.40}$$

$$\boldsymbol{\beta}_1 \equiv \boldsymbol{\beta}_{Z'}|_{\mathrm{lab}} = \frac{1}{1 + \boldsymbol{\beta}^*_{Z'} \cdot \boldsymbol{\beta}_0} \left[\frac{\boldsymbol{\beta}^*_{Z'}}{\gamma_0} + \boldsymbol{\beta}_0 + \frac{\gamma_0}{\gamma_0 + 1} \left(\boldsymbol{\beta}^*_{Z'} \cdot \boldsymbol{\beta}_0 \right) \boldsymbol{\beta}_0 \right], \tag{4.41}$$

$$\boldsymbol{\beta}^*_{\psi_2} = \frac{\mathbf{p}^*_{\psi_2}}{E^*_{\psi_2}} = \frac{\left[(m_{Z'}^2 - (m_{\psi_2} + m_{\psi_1})^2)(m_{Z'}^2 - (m_{\psi_2} - m_{\psi_1})^2) \right]^{1/2}}{m_{Z'}^2 - m_{\psi_1}^2 + m_{\psi_2}^2} \hat{\mathbf{n}}_2, \tag{4.42}$$

$$\boldsymbol{\beta}_2 \equiv \boldsymbol{\beta}_{\psi_2}|_{\mathrm{lab}} = \frac{1}{1 + \boldsymbol{\beta}^*_{\psi_2} \cdot \boldsymbol{\beta}_1} \left[\frac{\boldsymbol{\beta}^*_{\psi_2}}{\gamma_1} + \boldsymbol{\beta}_1 + \frac{\gamma_1}{\gamma_1 + 1} \left(\boldsymbol{\beta}^*_{\psi_2} \cdot \boldsymbol{\beta}_1 \right) \boldsymbol{\beta}_1 \right], \tag{4.43}$$

[2]The two-body decay of an unpolarised parent is isotropic in the CM frame, as noted in section 4.1.2.

where as usual $\gamma_i = (1-\beta_i)^{-1/2}$. The free paths ℓ_i are extracted from an exponential distribution with mean $\mu_i = \gamma_i \beta_i \tau_i$, where $\tau_i = 1/\Gamma_i$ is the mean lifetime. Once both $\mathbf{r}_2$ and $\boldsymbol{\beta}_2$ are obtained, we let `Mathematica` intersect the flight path of ψ_2, described by the equations

$$\frac{x - x_2}{\beta_{2x}} = \frac{y - y_2}{\beta_{2y}} = \frac{z - z_2}{\beta_{2z}}, \tag{4.44}$$

with the surface of a rectangular parallelepiped representing the active volume of ICARUS, placed according to the experimental geometry. The ratio between the number of valid intersections and the number of kaons we started with gives f_{det}.
As for the final factor in (4.38), f_{in} is the fraction of ψ_2 hitting the detector which actually decay inside, possibly leaving a signature. The probability of this happening is given by

$$P(\mathbf{r}_2, \boldsymbol{\beta}_2) = \exp\left(-\frac{L_{\text{in}}(\mathbf{r}_2, \hat{\boldsymbol{\beta}}_2)}{\gamma_2 \beta_2 \tau_2}\right) - \exp\left(-\frac{L_{\text{out}}(\mathbf{r}_2, \hat{\boldsymbol{\beta}}_2)}{\gamma_2 \beta_2 \tau_2}\right), \tag{4.45}$$

where L_{in} and L_{out} are the distances between $\mathbf{r}_2$ and the intersection points. Since the statistics at this point was very low, we decided to take the mean value of P as an estimate for f_{in}.

Benchmark points and results

A study of the parameter space $(\alpha_D, \varepsilon, m_{\psi_1}, n, \Delta_{21})$, where $n \equiv 1/r_1 = m_{Z'}/m_{\psi_1}$, was made to find which points could give higher statistics. In particular, the average ψ_2 decay position was considered, and compared with the centre of the detector. Encouraging results were found for $\alpha_D = 0.1$, which is high enough for efficient coannihilation in the early universe (as described in section 3.3). For the benchmark point given by $\varepsilon = 10^{-3}$, $m_{\psi_1} = 20$ MeV, $n = 20$, $\Delta_{21} = 0.1$, we found

$$R_{\text{BNB}} \simeq 2 \times 10^2/\text{year} \qquad R_{\text{NuMI}} \simeq 8 \times 10^2/\text{year}. \tag{4.46}$$

Figures 4.5 and 4.6 show the average decay distance from the centre of the detector, using respectively the BNB and the NuMI beam, with the different colours identifying 100 m bands. The warmest colour indicates that, choosing the parameters in that region, on average, the decay takes place within 100 m from the detector. The benchmark point is optimistically chosen within one such band (subfigures 4.5(a) and 4.6(b)). Incidentally, it is apparent that the ψ_2 decays resulting from the BNB secondaries are closer to the target than those associated to the NuMI beam, giving rise to larger bands in the figures. This can be attributed to the combination of two factors: the lower velocities of intermediate particles which diminish relativistic time dilation, and thus their lifetime, and the detector being closer to the target. This enhancement partially compensates the suppressions due to both the lower meson yield and the more restricted phase space.
We compare the results of this survey of the parameter space to the analysis of the thermal target in [49], by looking at the plots in subfigures 4.5(b-f) and 4.6(b-f). We superimposed the $y = y(m_{\psi_1})$ curves (the thermal target for $n = 2$) from figure 3.1 for clarity. It is apparent that the intersection with the $y = y(m_{\psi_1})$ curve (the thermal target) is very narrow, in the bottom left quadrant, and models with a lower mass difference Δ_{21} are more easily probed. Unless theoretical motivations are given for favouring that area, from our analysis it seems that matching ICARUS and thermal ranges is unlikely. Naturally, a more accurate job can be done by solving the Boltzmann equations and numerically

comparing the thermal target hypersurface with the preferred ICARUS range.
A further refinement could be finding the energy spectrum for the decay products and comparing it to the energy threshold of the detector and background signals. We are also neglecting secondary collisions in the targets, which can significantly enhance the meson yield. Another possibility of expanding our analysis is considering the stopped kaons at the end of the decay pipe, which would give tracks in a distinct direction.

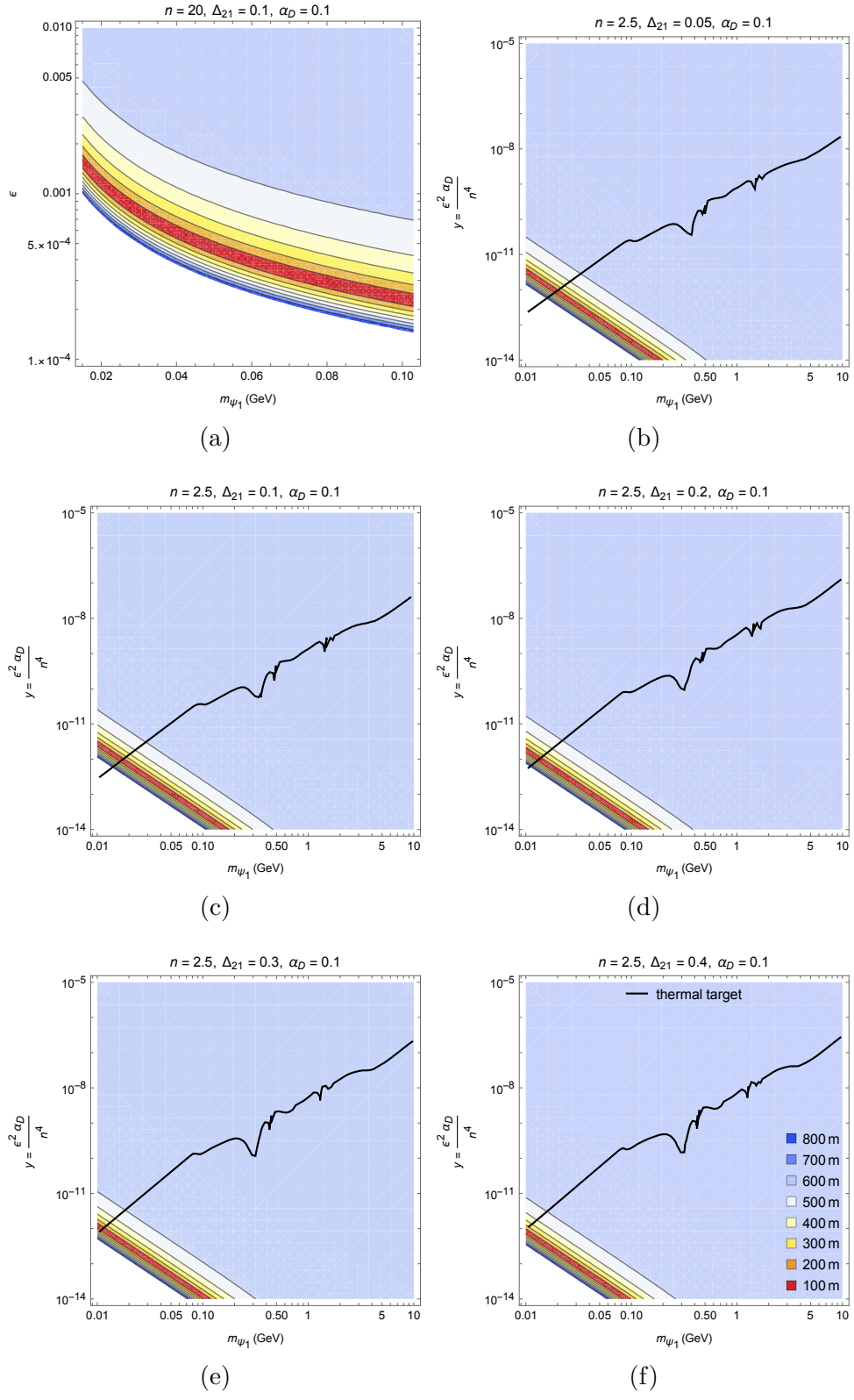

Figure 4.5: Average distance between the ψ_2 decay events and the centre of the ICARUS detector, using the Booster Neutrino Beam (BNB). Coloured contours delimit 100 m regions up to 800 m, with the warmest colour denoting decays within 100 m from ICARUS. Benchmark used for simulation (a) and thermal benchmarks (b-f), with the $n = 2.5$ thermal target curve reconstructed from [49].

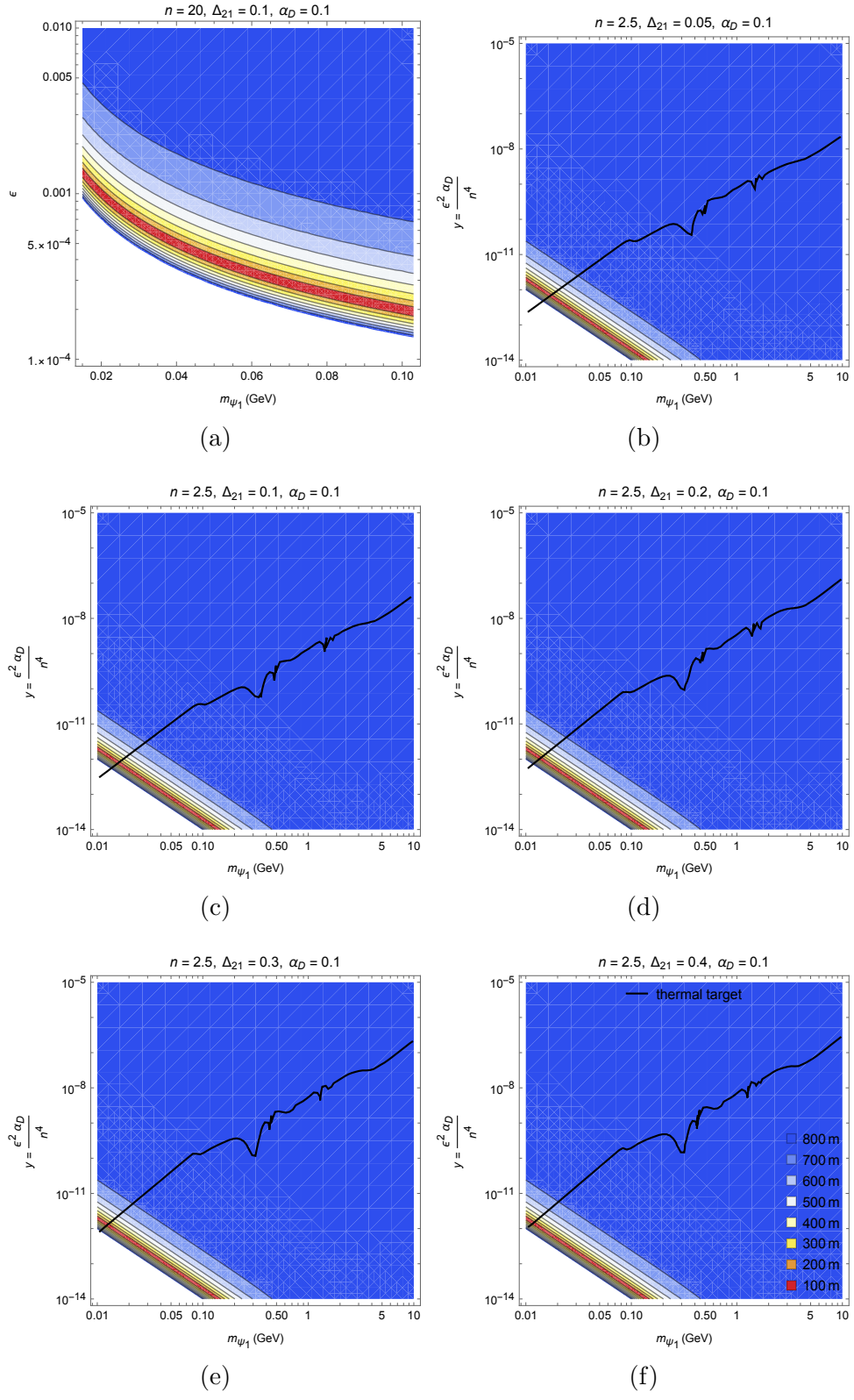

(a) (b) (c) (d) (e) (f)

Figure 4.6: Average distance between the ψ_2 decay events and the centre of the ICARUS detector, using the Neutrino at the Main Injector (NuMI) beam. Coloured contours delimit 100 m regions up to 800 m, with the warmest colour denoting decays within 100 m from ICARUS. Benchmark used for simulation (a) and thermal benchmarks (b-f), with the $n = 2.5$ thermal target curve reconstructed from [49].

Conclusions

Throughout this work, we have presented a collection of non-minimal dark sector models and analysed its multiple applications. We reviewed the sub-GeV dark sector solution to the problem of dark matter, its theoretical motivations and its current and possible experimental tests, observing that, in its various realisations, it can also provide explanation to several other unsolved problems: neutrino masses through the seesaw mechanism, baryon asymmetry through leptogenesis, low energy anomalies.
In particular, the semi-visible dark photon model, motivated by the existing experimental bounds on visible and invisible dark photon events, was shown to provide both a viable DM candidate and a seesaw mechanism that explains the measured mass-squared differences for atmospheric and solar neutrinos. This is achieved by introducing new heavy Majorana fermions, also in the MeV-GeV scale and postulating a Z_2 or lepton parity symmetry for some of them, while letting others interact via Yukawa terms with the SM neutrinos, which become neutrino mass terms upon spontaneous symmetry breaking. We showed how one can obtain perturbative Yukawa couplings, in an inverted seesaw scenario, starting from our experimental knowledge of neutrino masses (with the hypothesis that the lightest mass eigenstate is actually massless) and working bottom-up using Casas-Ibarra parametrisation.
The semi-visible decay of the dark photon was then examined quantitatively and embedded in a realistic context. In the models considered, it consists of the two stages $Z' \to \psi_2\psi_1$, $\psi_2 \to \psi_1\ell^-\ell^+$, where the $\ell^\pm$ constitute a SM lepton-antilepton pair that can generate a signal in a particle detector. After calculating the decay rates, we ran a simulation of the production, decay and detection at ICARUS, in its current operation as part of the Fermilab short-baseline neutrino program. The neutral mesons produced in the fixed-target collisions may indeed decay to dark photons, leaving a distinct signature. Using K_L^0 mesons generated with `Pythia` and modelling the propagation and decay chain with `Python` and `Mathematica` scripts, a sample of events in the LArTPC was computed. From that, a total number of about 10^3 events per year was deduced for the considered benchmark point, considering both the NuMI beam and the BNB collisions. If one is to interpret the lighter state ψ_1 as inelastic DM, the region in the parameter space corresponding to the observed abundance was shown to have a rather small overlap with the range available for observations at ICARUS, hinting at this scenario being fine-tuned. However, deeper analysis is needed to deem iDM tests as too fortuitous for this kind of experiment. The Monte Carlo simulation itself is intended to be refined and expanded for other present and upcoming beam dump experiments.

Acknowledgements

I would like to express my sincere gratitude to all the people who made this work possible. I am deeply thankful to prof. Silvia Pascoli for her kind, masterful guidance, and for having entrusted me with a work that pushed me beyond my limits and gave me far more confidence in facing original research. A huge thank you goes to dr. Alessandro Granelli for his essential help in filling the gaps in my knowledge, for his patience as co-supervisor, and for the always inspiring scientific conversations. I would also like to thank Jaime Hoefken Zink for his time, suggestions and encouragement.
Naturally, many other factors concurred to me getting to this point, and I have to mention how grateful I am for the new friendships I had the honour of forming here in Bologna, as well as for the warmth sent me from my family and friends in Naples and scattered around the world.

Bibliography

[1] F. Zwicky. *Helv. Phys. Acta*, 6:110–127, 1933.

[2] V. C. Rubin and W. K. Ford Jr. *Astrophys. J.*, (159):379, 1970.

[3] D. Clowe, M. Bradač, A. H. Gonzalez, M. Markevitch, S. W. Randall, C. Jones, and D. Zaritsky. *Astrophys. J.*, 648(L109-L113), 2006.

[4] N. Aghanim *et al.* [Planck Collaboration]. *Astron. Astrophys.*, (A6):641, 2020.

[5] M. Davis S. D. M. White, C. S. Frenk. *Astrophys. J.*, 274:L1–L5, 1983.

[6] G. Bertone and T. M. P. Tait. *Nature*, 562:51–56, 2018.

[7] S. Tremaine and J. E. Gunn. *Phys. Rev. Lett.*, 42(6):407–410, 1979.

[8] C. R. Argüelles, E. A. Becerra-Vergara, J. A. Rueda, and R. Ruffini. *Universe*, 9(197), 2023.

[9] G. Gilmore, M. I. Wilkinson, R. F. G. Wyse, J. T. Kleyna, A. Koch, N. W. Evans, and E. K. Grebel. *Astrophys. J.*, 663:948–959, 2007.

[10] E. W. Kolb and M. S. Turner. *The early universe.* Westview Press, 1990.

[11] S. Dodelson. *Modern cosmology.* Academic Press, 2003.

[12] B. W. Lee and S. Weinberg. *Phys. Rev. Lett.*, 39:165.

[13] M. W. Goodman and E. Witten. *Phys. Rev. D*, 31(12):3059–3063, 1985.

[14] A. K. Drukier, K. Freese, and D. N. Spergel. *Phys. Rev. D*, 33(12):3495–3508, 1986.

[15] M. Lisanti. arXiv:1603.03797v2 [hep-ph], 2016.

[16] T. Piffl *et al. Astron. Astrophys.*, 562(A91), 2014.

[17] R. Bernabei *et al. J. Phys.: Conf. Ser.*, 203(012003), 2010.

[18] Z. Ahmed *et al.* [CDMS Collaboration]. *Phys. Rev. Lett.*, 106(131302), 2011.

[19] T. Lin. arXiv:1904.07915v1 [hep-ph], 2019.

[20] R. Essig, T. Volansky, and T. Yu. *Phys. Rev. D*, 96(043017), 2017.

[21] P. Agnes *et al.* [DarkSide Collaboration]. *Phys. Rev. Lett.*, 121(111303), 2018.

[22] M. Ibe, W. Nakano, Y. Shoji, and K. Suzuki. *JHEP*, 2018(194), 2018.

[23] R. Essig, M. Fernández-Serra, J. Mardon, A. Sato, T. Volansky, and T. Yu. *JHEP*, 2016(46), 2016.

[24] S. Knapen, T. Lin, M. Pyle, and K. M. Zurek. *Phys. Lett. B*, 785:386–390, 2018.

[25] D. Hooper. arXiv:1812.02029 [hep-ph], 2018.

[26] T. R. Slatyer. arXiv:1710.05137 [hep-ph], 2017.

[27] C. A. Argüelles, A. Diaz, A. Kheirandish, A. Olivares-Del-Campo, I. Safa, and A. C. Vincent. *Rev. Mod. Phys.*, 93(035007), 2021.

[28] O. Adriani *et al.* [PAMELA]. *Nature*, 458:607–609, 2009.

[29] M. Aguilar *et al.* [AMS Collaboration]. *Phys. Rev. Lett.*, 110(141102), 2013.

[30] P. Yin, Z. Yu, Q. Yuan, and X. Bi. *Phys. Rev. D*, 88(023001), 2013.

[31] M. Aguilar *et al.* [AMS Collaboration]. *Phys. Rev. Lett.*, 110(141102), 2013.

[32] A. Cuoco, M. Krämer, and M. Korsmeier. *Phys. Rev. Lett.*, 118(191102), 2017.

[33] M. G. Aartsen et al. *JCAP*, 2016(022), 2016.

[34] M. D. Schwartz. *Quantum Field Theory and the Standard Model*. Cambridge University Press, 2014.

[35] P. A. Zyla *et al.* [Particle Data Group]. *Prog. Theor. Exp. Phys.*, 2020(8):671–674, 2020.

[36] Y. Fukuda *et al.* [Super-Kamiokande Collaboration]. *Phys. Rev. Lett.*, 81(8):1562, 1998.

[37] Q. R. Ahmad *et al.* [SNO Collaboration]. *Phys. Rev. Lett.*, 87(7), 2001.

[38] M. Aker *et al.* [KATRIN Collaboration]. *Nat. Phys.*, 18:160–166, 2022.

[39] A. Ibarra, E. Molinaro, and S. T. Petcov. *JHEP*, 2010(108), 2010.

[40] J. A. Casas and A. Ibarra. *Nucl. Phys.*, 618(1-2):171–204, 2001.

[41] B. Holdom. *Phys. Lett. B*, 166(2):196–198, 1986.

[42] A. M. Abdullahi, M. Hostert, D. Massaro, and S. Pascoli. *Phys. Rev. D*, 108, 2023.

[43] D. Smith and N. Weiner. *Phys. Rev. D*, 64(043502), 2001.

[44] Z. Ahmed *et al.* [CDMS Collaboration]. *Phys. Rev. D*, 83(112002), 2011.

[45] A. M. Abdullahi, M. Hostert, and S. Pascoli. *Phys. Lett. B*, 820(136531), 2021.

[46] A. Filimonova, S. Junius, L. Lopez Honorez, and S. Westhoff. *JHEP*, 06(048), 2022.

[47] E. Ma. *Phys. Rev. Lett.*, 115(011801), 2015.

[48] I. Esteban, M. C. Gonzalez-Garcia, M. Maltoni, Thomas Schwetz, and A. Zhou. *JHEP*, 09(178), 2020.

[49] M. Duerr, T. Ferber, C. Hearty, F. Kahlhoefer, K. Schmidt-Hoberg, and P. Tunney. *JHEP*, 2020(39), 2020.

[50] E. Izaguirre, Y. Kahn, G. Krnjaic, and M. Moschella. *Phys. Rev. D*, 96(055007), 2017.

[51] P. A. Zyla *et al.* [Particle Data Group]. *Prog. Theor. Exp. Phys.*, 2020(8):1358, 2020.

[52] B. Batell, M. Pospelov, and A. Ritz. *Phys. Rev. D*, 80(095024), 2009.

[53] A. Denner, H. Eck, O. Hahn, and J. Küblbeck. *Phys. Lett. B*, 291(3):278–280, 1992.

[54] S. Amerio *et al.* [ICARUS collaboration]. *Nucl. Instrum. Methods Phys. Res., Sect. A*, 527:329–410, 2004.

[55] P. Abratenko *et al.* [ICARUS collaboration]. *Eur. Phys. J. C*, 83(467), 2023.

[56] B. Batell, J. Berger, and A. Ismail. *Phys. Rev. D*, 100(115039), 2019.

[57] C. Bierlich *et al. A comprehensive guide to the physics and usage of PYTHIA 8.3.* arXiv:2203.11601 [hep-ph] [DOI:10.21468/SciPostPhysCodeb.8], 2022.

[58] C. Bierlich, G. Gustafson, L. Lönnblad, and H. Shah. *JHEP*, 2018(134), 2018.

[59] P. A. Zyla *et al.* [Particle Data Group].

[60] Y. Cui, D. E. Morrissey, D. Poland, and L. Randall. *JHEP*, 05(076), 2009.

[61] C. Antel *et al. Eur. Phys. J. C*, 83(1122), 2023.

[62] P. Agrawal *et al. Eur. Phys. J. C*, 81(1015), 2021.

[63] M. Fabbrichesi, E. Gabrielli, and G. Lanfranchi. *The Physics of the Dark Photon.* Springer Cham, 2020.

[64] P. Ballett, T. Boschi, and S. Pascoli. *JHEP*, 2020(111), 2020.

[65] P. Minkowski. *Phys. Lett. B*, 67(4):421–428, 1977.

[66] P. Ballett, M. Hostert, and S. Pascoli. *Phys. Rev. D*, 101, 2020.

[67] H. Zhang. *Phys. Lett. B*, 714(2-5):262–266, 2012.

[68] S. Pascoli. *CERN Yellow Rep. School Proc. 6*, pages 213–259, 2019.